Numerical modelling of slope damage in large, slowly moving rockslides: Insights from the Downie Slide, British Columbia, Canada

Numerical modelling of slope damage in large, slowly moving rockslides: Insights from the Downie Slide, British Columbia, Canada.

Davide Donati[1]* (ORCiD: 0000-0003-4083-5910); Doug Stead[1]; Thomas W. Stewart[2]; Julia Marsh[2]

1 Simon Fraser University, Department of Earth Sciences, Burnaby, British Columbia, Canada

2 BC Hydro and Power Authority, Vernon, British Columbia, Canada

* Corresponding author:

Davide Donati

Simon Fraser University

8888 University Drive V5A 1S6 Burnaby, British Columbia, Canada

TASC 1, Department of Earth Sciences, Room 7001

email: davide_donati@sfu.ca

Funding: This work was supported by the Natural Sciences and Engineering Research Council of Canada [grant number RGPIN 05817] and Forestry Renewal British Columbia Endowment funds provided to Doug Stead.

Conflict of Interest: The authors declare that they have no conflict of interest.

Author contributions: Davide Donati: Conceptualization; Investigation; Formal analysis, Writing – original draft. Doug Stead: Conceptualization; Writing – Review and Editing; Supervision; Funding acquisition. Thomas W. Stewart: Resources; Writing – Review and Editing; Julia Marsh: Resources; Writing – Review and Editing.

Abstract

The deformation of rock slopes is associated with the formation and accumulation of internal and external features (such as tension cracks, rock mass bulging and dilation, rockfall, etc.) that can be comprehensively referred to as “slope damage”. In this paper, we use a 3D distinct element numerical modelling approach to investigate the role of shear zone morphology and groundwater pressure on the displacement and slope damage accumulation at the

Downie Slide, a large, extremely slowly moving rockslide in British Columbia (Canada). First, we briefly review the external slope damage features that can be observed in an airborne laser scanner (ALS) dataset, allowing four slope damage domains (upper, central, northern, and southern domain) to be interpreted within the slide area, based on the orientation and type of features. Using the same ALS dataset we construct a 3D model of the present-day slope, explicitly including the two shear zones along which displacements occur, in order to investigate their role in the later stage of the landslide evolution. We assign a strain-softening constitutive model to the slide body, in order to account for the decrease in material properties due to damage accumulation. Virtual inclinometers are also implemented in the model, allowing for the comparison of simulated and observed displacement direction along the shear zones. The progressive deformation and failure of the slope is then simulated both assuming dry and wet conditions, in order to examine the role of pore water pressure, and the morphology of the upper and lower shear zones on the magnitude, orientation, and distribution of displacements. For each numerical model, the simulated slope damage features are recorded, by analyzing the zone volumetric strain and failure state, and compared with the type and orientation of features observed in each of the interpreted slope damage domains, thus allowing the numerical results to be better constrained and validated. It is clearly demonstrated that the orientation and distribution of slope damage and displacements observed in both the surface ALS and the subsurface borehole inclinometer data can be well reproduced in the 3D numerical models. Numerical modelling results show that the principal factor controlling the spatial distribution of slope damage at the Downie Slide is the morphology of the lower shear zone, whereas a negligible role is played by the upper shear zone morphology. We also observe that models incorporating a groundwater table display larger displacements, without significant effects on the orientation and distribution of simulated slope damage. This paper demonstrates that an analysis of slope damage is very important for understanding the mechanisms underlying the behavior of large landslides and should be a fundamental step in the comprehensive characterization of any major slope failure.

Keywords: slope damage, Downie Slide, numerical modelling, distinct element method, airborne laser scanning

1 Introduction

The stability and evolution of high rock slopes is controlled by several important factors, including geologic and lithological features that combine to define the global strength of a rock slope. Structural and lithological features, such as faults, folds, rock mass jointing, foliation, and bedding may form release surfaces, along which volumes of the rock mass may slide or detach (Saintot et al. 2011; Stead and Wolter 2015). Many major rockslides have been at least partially controlled by inherited geological structures or lithology. The 1963 Vajont Slide displaced on thin clay-rich layers along a structural, chair-shaped basal surface, and the failed volume was bounded by persistent faults (Semenza and Ghirotti 2000). The failure of the 1965 Hope Slide was promoted by rock mass jointing and structural damage associated with faults and shear zones (Brideau et al. 2005). Badger (2002) illustrated the effects of fracturing in anticlinal folds on the stability of rock slopes, using conceptual drawings and field observations, showing that tensile cracking, perpendicular to the rock mass bedding, may act either as basal or rear rupture surfaces and provide kinematic freedom to potentially unstable blocks. An excellent example is represented by the 1903 Frank Slide, in which basal and rear kinematic freedom was provided by geological structures associated with the Turtle Mountain syncline (Humair et al. 2013). Structural material heterogeneities may also contribute to define the style of deformation of large slope instabilities. Many active, slowly moving rockslides, such as the Aknes Rockslide (Norway, Ganerød et al. 2008) and the Campo Vallemaggia rockslide (Switzerland, Bonzanigo et al., 2007) are actively displacing along sliding surfaces parallel to foliation or schistosity. Structural and geological features at various scales (ranging from significant tectonic lineaments to local variations in rock mass quality) may also promote slope instability indirectly, by decreasing the strength of the rock mass and increasing the permeability within the slope (Ambrosi and Crosta 2006; Agliardi et al. 2013b). It is clear there is a need to characterize rock slopes not only from a geotechnical but also from a structural geology perspective (Stead and Wolter 2015).

In addition to the aforementioned geological factors that control the location and volume of the potential instability, the action of exogenic (e.g., alteration, weathering, rainfall, snowmelt) and endogenic processes (e.g., isostasy, volcanism, earthquakes) gradually weaken the slope, causing a progressive decrease in stability (Whalley 1974; Leith 2012). This process, known as “progressive failure”, is often accompanied by the formation of internal and surface features induced by the slope deformation that are referred to as “slope damage” (Stead and Eberhardt 2013). Extensional features, such as uphill and downhill facing scarps, double crest ridges, normal faults, tension cracks, closed depressions, and grabens are all slope damage features commonly observed in deep-seated slope deformations (Agliardi et al. 2013a; Jaboyedoff et al. 2013), together with buckling, folds, and reverse faulting (Chigira 1992; Stead and Eberhardt 1997). The progressive rock mass weakening associated with the accumulation of slope damage may facilitate the formation of release surfaces, enhancing the kinematic freedom and mobility of rock slopes (Adhikary et al. 1997; Agliardi et al. 2013b).

The investigation of slope damage can provide insights on the mechanisms and processes that control (or controlled) the slope deformation and failure. Wolter et al. (2014) employed an engineering-geomorphological

approach to investigate the pre- and post-failure topography of the Vajont slide, and highlighted the role of endogenic and exogenic factors on the evolution of the failure. Paronuzzi and Bolla (2015) also investigated Vajont slide deposit in order to characterize the ductile and brittle features (referred to as gravity-induced rock mass damage) that developed during the failure. The characterization of slope damage can also provide information on the temporal evolution of the instability. Agliardi et al. (2009) employed radiocarbon analyses to characterize the age of trench infilling, in order to reconstruct the chronological evolution of the Mt. Watles deep-seated slope gravitational displacement (DSGSD) in Northern Italy. Carbonel et al. (2013) performed stratigraphic and radiometric analyses to distinguish between tectonic and geomorphic features along a high slope in Northern Spain. Hermanns et al. (2015) employed cosmogenic dating to investigate the age of a slope deformation in the south face of the Aconcagua Mountain (Argentina). Oppikofer et al. (2017) also used cosmogenic dating to investigate and reconstruct the progressive displacement of the Vollan DSGSD (Norway). Using historic aerial photographs to map slope damage features, Clayton et al. (2017) interpreted the failure mechanism of the Mitchell Creek Landslide, highlighting the role of the glacial retreat in the evolution of the slope instability. Donati et al. (2020) investigated the slope damage at the Ten Mile slide site, in British Columbia (Canada) using a series of airborne laser scanner datasets (ALS), and highlighted the geomorphic control of the slope damage accumulating at the slope surface.

Although slope damage is recognized as a critical factor controlling and promoting the occurrence of slope instability, the mechanisms and processes through which it accumulates, and the effects on the slope stability are seldom addressed in numerical modelling analyses. Moore et al. (2011) investigated the role of ground-shaking in the stability of the Randa rockslides. Preisig et al. (2016) used numerical modelling to reproduce the displacement and progressive damage accumulation due to hydromechanical fatigue and seasonal water table variations in a deep-seated landslide. Riva et al. (2018) analysed the progressive accumulation of damage in a DSGSD initiated by glacial retreat in the Italian Alps.

In this paper, we use a numerical modelling approach to investigate the Downie Slide, a massive, active, composite, extremely slowly moving rockslide in British Columbia, Canada. The objective of the simulation is to identify the factors controlling the orientation, type, and spatial distribution of slope damage features that can be observed at the slope surface. Additionally, this analysis will demonstrate the effectiveness of using slope damage features as constraint for numerical simulation results, potentially enhancing the reliability of numerical modelling of slopes where monitoring data is not readily available.

2 Overview of the Downie Slide

2.1. Geological, structural, and hydrogeological setting

The Downie Slide has been classified as a massive, active, composite, extremely slowly moving rockslide (Kalenchuk et al. 2009). It is located in south-eastern British Columbia (Canada), along the western shore of the

Revelstoke reservoir (Figure 1a,b). The reservoir was impounded in 1984 after the construction of the Revelstoke dam by BC Hydro, 70 km south of the slide area along the Columbia River Valley (Imrie and Moore 1993). The elevation of the Columbia River before the reservoir impoundment was 507 m a.s.l., which roughly coincided with the daylighting elevation of the basal sliding surface. After the construction of the dam, water level increased to 573 m a.s.l., submerging the toe of the slide.

The Downie Slide has a surface area of about 9 km^2, and extends 2.4 km in the north-south direction and 3.2 km in the east-west direction, between ground surface elevations of 500 m and 1520 m a.s.l. The slide is bounded, to the south and west, by sub-vertical scarps up to 125 m high, whereas no prominent scarps can be observed along most of the northern boundary. The slide volume has been estimated between 1.0 billion m^3 (Donati 2019) and 1.5 billion m^3 (Piteau et al. 1978).

The most prominent structural feature in the Downie Slide area is the Columbia River Fault, CRF, which dips 20 to 30° towards the east. The CRF was generated, in the Middle-Late Jurassic, by overthrusting of the Selkirk Allochthon over the Monashee Complex, to the west and east respectively of the CRF (Brown and Read 1983). The CRF is bounded by a cataclastic zone, about 1000 m wide, that predominantly affects the eastern slope of the valley (Figure 1c; Brown and Psutka, 1980). Although the CRF played a key-role in defining the structural setting of the area, no conclusive evidence was found that this geological structure was directly related to the initiation and development of the Downie Slide (Brown and Psutka, 1980).

The Downie Slide comprises a succession of mica schists, mica gneisses, and quartzite gneiss that are part of Proterozoic to Lower Paleozoic Monashee Complex (Brown and Psutka 1980; Brown and Read 1983). The material is characterized by a prominent foliation that dips towards the east at an angle of about 20°, sub-parallel to the slope surface, and provides weakness planes along which displacements occur (Brown and Psutka 1980).

Geological investigations, including geophysical surveys and borehole drilling, evidenced that the slide is displacing along two sub-parallel shear zones (Imrie et al. 1992), referred to as lower and upper shear zones (USZ and LSZ, respectively, Figure 1d). Monitoring data show that displacement rates are not homogeneously distributed across the slide volume. At depth, borehole inclinometer surveys recorded movements up to 1.7 and 3.2 mm/year along the USZ and LSZ, respectively. Rates of up to 16 mm/year have also been observed near the toe, but these are limited to a shallow layer in colluvial material. Ground surface displacements, monitored using periodical GPS monument surveys, vary between 1 and 58 mm/year, with a peak of 174 mm/year in the northern part of the toe (BC Hydro 2010).

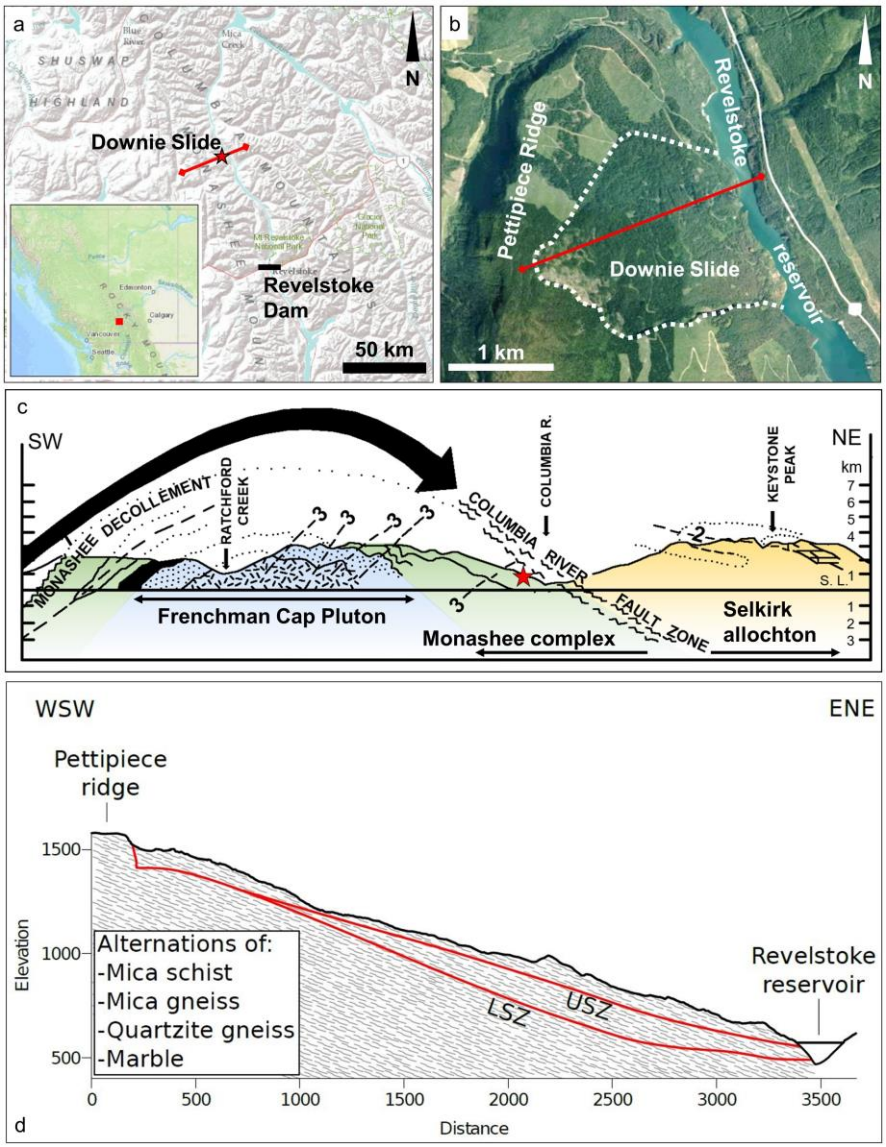

Figure 1 **Geographic and geological overview of the Downie Slide. a: location of the study area in western Canada. The location of the Revelstoke Dam is also indicated. Solid line identifies the geological section in panel c; b: 2003 satellite image (from Google Earth) of the Downie Slide. Note the Revelstoke reservoir submerging the toe of the slide. Solid line represents the trace of the section shown in panel d; c: geological section through the study area and the Downie Slide. Note the interpreted overthrust of the Selkirk Allochton along the Monashee Decollement and the inferred thickness of the Columbia River Fault zone. Numbers 2 and 3 mark fold axes of the relative secondary and tertiary tectonic deformation phases that affected the region (modified from Read and Brown, 1981) d: conceptual geological section of the Downie Slide, showing the foliation orientation, the lower shear zone (LSZ) and the upper shear zone (USZ).**

The hydrogeological setting comprises several independent aquifers, located at varying depth within the slide, which are a primary factor controlling the displacement rates across the slide area. Between 1973 and 1982, prior to the impoundment of the Revelstoke reservoir, two drainage adits were excavated within the Downie Slide, in order to increase the stability through the reduction of the piezometric head along the shear zones. In the lower slope

the water table was lowered of up to 152 m, resulting in a decrease in displacement rates from 10 mm/year (pre-reservoir rates along the LSZ) to the present-day rates (BC Hydro 2010).

The Downie Slide initiated between 7,900 and 10,000 years ago, during or shortly after the glacial retreat in the Columbia River Valley (Piteau et al., 1978; Stantec Inc 2009), and a total displacement of about 300 m was estimated (Stantec Inc. 2009). It has been suggested that the Columbia River was progressively pushed against its eastern bank by the slide, which never blocked the valley, nor evolved into a rapid instability (Stantec Inc. 2009). Such a deformation process resulted in the narrowing of the Columbia River, particularly at two prominent knobs located at the southern and northern boundaries of the slide area (referred to as south knob and north knob, respectively), where rapids formed due to the increase in flow velocity.

Based on geomorphic and structural considerations, various sub-divisions have been proposed for the Downie Slide. Piteau et al. (1978) proposed a sub-division of the slide area into five domains. Based on field reconnaissance and ALS interpretation, Stantec Inc. (2009) and Kalenchuk et al. (2013a) proposed sub-division of the slide area into 8 and 13 domains, respectively. In this paper, we refer to the sub-division by Westin (2017), which proposed 12 domains, interpreted using a mixed structural-geomorphic ALS approach in a GIS environment.

2.2. Slope damage at the Downie Slide

The external slope damage at the Downie Slide was investigated using an ALS dataset. Internal damage was also preliminarily investigated using sub-surface data, including borehole inclinometer, piezometer logs, and underground terrestrial laser scanning (TLS; Donati, 2019; Westin, 2017). Based on the orientation, spatial distribution, and size of the slope damage features mapped on the ALS dataset, the slide area was divided into four slope damage domains: upper distributed slope damage domain, central undamaged domain, northern slope damage domain, and southern slope damage domain (Figure 2a). The upper distributed slope damage domain is characterized by a hummocky morphology generated by the progressive retrogression of the upper headscarp (Kalenchuk et al. 2013a; Westin 2017). The central undamaged domain is characterized by a smooth, relatively undisturbed surface with no prominent slope damage features. In the northern slope damage domain, extensive surface cracking can be observed, with fractures, up to 20 m wide, oriented in north-south and northeast-southwest directions. The southern slope damage domain is affected by east-west tensile cracks and grabens, as well as north-south oriented counterscarps in the lower slope (Figure 2a). For a detailed description of each single slope damage domain, the reader is referred to Donati (2019).

External and internal slope damage are strongly correlated to the morphology and changes in aspect of the LSZ, which was constructed by interpolating, using a Kriging approach, the shear zone depth observed at the location of 35 borehole and inclinometer logs (Donati, 2019). The LSZ displays a bi-planar configuration, as the gradient at the toe of the slope is lower (less than 15°) than the medium and upper slope (up to > 30°, Figure 3a). As a result, the progressive displacement caused the accumulation of internal slope damage within the transition zone at

the interface between the active (i.e., upper) and passive (i.e., lower) blocks. The LSZ is also characterized by a bi-planar morphology in the north-south direction, as the northern part of the shear zone dips towards the east, while the southern part dips towards the north-east (Figure 3b, Donati 2019). Compared to the LSZ, the USZ appears to be characterized by a more homogeneous surface, with more limited changes in dip direction and slope angle (Figure 3c,d). The complex geometric configuration of the LSZ is likely related to a possible geological structure that crosses the slide area, intersecting the headscarp (generating a prominent knob clearly visible in the ALS dataset), and forming the Fissure Creek Valley to the west of the slide area (Fissure Creek Structure in Figure 2c). The damage zone surrounding this geological structure is thought to be the cause of a localized decrease in rock mass quality, which is reflected in an increase in surface roughness observed in the central undamaged domain (Figure 2b), and the presence of a distributed slope damage zone in the northern slope damage domain (Figure 2a). The long-term displacement along the LSZ and USZ also caused the accumulation of internal slope damage. Borehole logs and photographs evidenced that the rock mass forming the shear zones is intensely altered, fractured, and sheared. The thickness of such highly damaged zone in the LSZ and the USZ is up to 62 m and 21 m, respectively, with peak values observed in the lower slope. However, borehole inclinometer logs show that displacements at depth are concentrated within a 1-m thick layer in both the LSZ and USZ. Such thickening may have resulted from a combination of various factors, including the damage accumulation in the transition zone, the displacement along a potentially undulated surface, and the possible activity, in the past of different or multiple sliding surfaces.

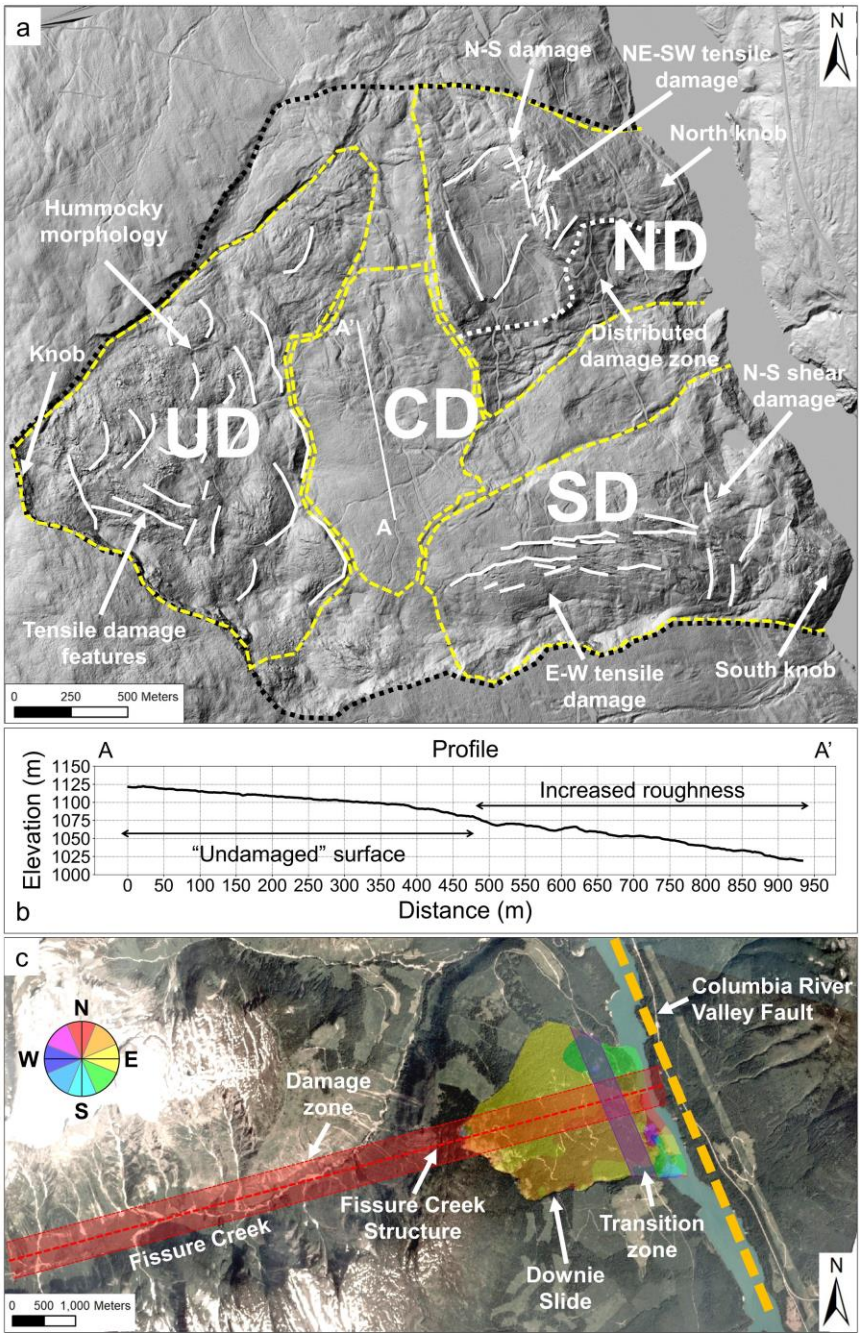

Figure 2 **Overview of the external and internal slope damage at the Downie Slide. a: external slope damage domains identified in the ALS dataset. UD: upper distributed slope damage domain; CD: central undamaged domain; ND: northern slope damage domain; SD: southern slope damage domain. Note the varied orientation and type of slope damage features across the slope damage domains, the knob along the upper headscarp, and the south and north knobs at the toe of the slide. The solid line in CD marks the profile trace shown in b; b: N-S profile along the CD domain. Note the increase in roughness in the northern part, interpreted as the result of a lower rock mass quality and higher erodibility; c: factors controlling internal damage at the Downie Slide. Note the alignment between Fissure Creek, the knob in the upper headscarp, and the change in aspect of the LSZ, suggesting the presence of a structural damage zone. In the lower slope, transition zone and vicinity to the Columbia River Valley Fault likely enhance internal damage.**

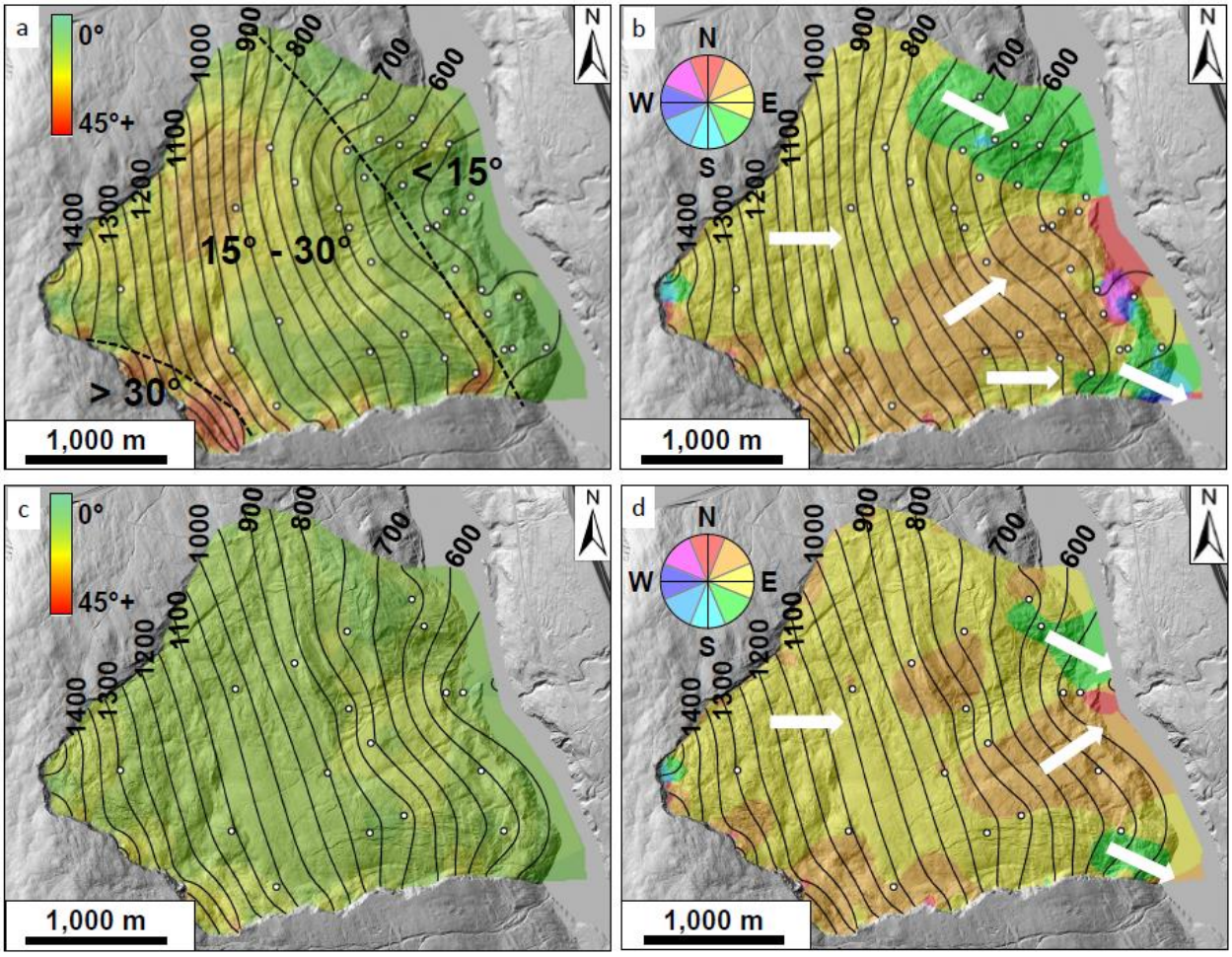

Figure 3 **Morphology of the upper and lower shear zones constructed by interpolation of borehole data (white circles). a: slope map of the LSZ. Note the decrease in steepness of the LSZ in the lower part of the slope. b: aspect map of the LSZ. White arrows show the average orientation of the planes composing the shear zone. c: slope map of the USZ. d: aspect map of the USZ.**

3 Numerical modelling of the Downie Slide

In this work, three-dimensional numerical modelling was performed to investigate the factors that are controlling the evolution of slope damage at the Downie Slide. In particular, the influence of shear zone morphology, structural and geomorphic domain sub-division, and ground water conditions on the development of internal and external slope damage was investigated. The spatial distribution, orientation, and type of external slope damage observed in the ALS dataset were compared with the results from the numerical analysis. It was noted that using a distinct element method, coupled with a strain-softening constitutive model, slope damage features can be reproduced in a three-dimensional numerical model, providing an additional tool for constraining numerical analysis. The numerical model analyzes a slope that is representative of the final evolution stages and present-day conditions for the Downie Slide (in terms of slope topography, slide boundaries, shear zone morphology, ground water table,

rock mass properties), and therefore represents a prototype for forward modelling. Such approach was elaborated in collaboration with the Dam Safety branch of BC Hydro, in order to identify areas where additional borehole data collection, planned for the next few years, should concentrate to enhance understanding of mechanisms controlling the slide behavior.

3.1. Construction of the three-dimensional model of the Downie Slide

Since the slide volume can be divided into discrete domains, a three-dimensional distinct element method approach was used for the numerical analysis, and the code 3DEC 5.2 (Itasca Consulting Group 2016a) was employed. In the distinct element method, the rock mass is modelled as an assembly of discrete blocks that may slide, rotate, and completely detach from each other.

The numerical analysis was undertaken considering the present-day slope morphology as the initial model condition. The model geometry was created in Rhinoceros 5 (Robert McNeel & Associates 2015) using the ALS dataset. To avoid boundary effects in proximity of the slide area, the model area was extended, using a NASA SRTM dataset (NASA-NGA 2014). The final model geometry covers a surface area of 5.3 km by 5.3 km (Figure 4). The LSZ and USZ, reconstructed from borehole and inclinometer log data as described in Donati (2019), were implemented in the 3DEC model. Finally, using Griddle (Itasca Consulting Group 2016b) a tetrahedral volumetric mesh was exported in a format readable in 3DEC.

The Downie Slide area was sub-divided into eight deformable blocks divided by vertical boundaries, roughly based on Westin (2017), in order to provide kinematic freedom to the different parts of the slide. The choice of vertical boundaries in this analysis is for 3D model simplicity and is justifiable as there are currently no existing data on the sub-surface dip of domain boundaries. It is currently unclear whether the block boundaries are structural in origin or formed as a result of the slope deformation, or possibly a combination of both. From the upper to the lower slope, the slide blocks are: upper hummocks, talus, mid plain, mid hummocks, south knob, channelized lower, upper north knob, and lower north knob (Figure 4). Kalenchuk et al. (2013) and Westin (2017) suggested that the upper blocks (namely upper hummocks and talus) formed through the progressive retrogression and erosion of the head scarp of the Downie Slide. The irregular ground surface of the upper slope suggests that large rock blocks progressively detached and failed, “filling the gap” created by the displacing slide and generating a prominent hummocky morphology. It is unlikely that such an accumulation mechanism allowed a foliation-parallel USZ to form, and it was therefore decided not to implement the USZ in these blocks. A strain-softening constitutive criterion was assumed for the slide material, in order to simulate the decrease in rock mass properties caused by the accumulation of internal and external slope damage. Observed in-place stable areas within the large-scale model (i.e., outside of the slide area) were assumed to be elastic. Rock mass properties were obtained from Kjelland (2004) and Kalenchuk et al. (2012), and were derived from numerous investigations and material testing programs by BC Hydro. In this investigation, residual strength properties for the strain-softening model are assigned after a plastic

strain of 2%. This value is within the range used in previous numerical analyses (0.2% to 6%) to simulate rock mass strength softening (Hajiabdolmajid and Kaiser 2002; Badr et al. 2003; Andrieux et al. 2004; Zipf 2007).

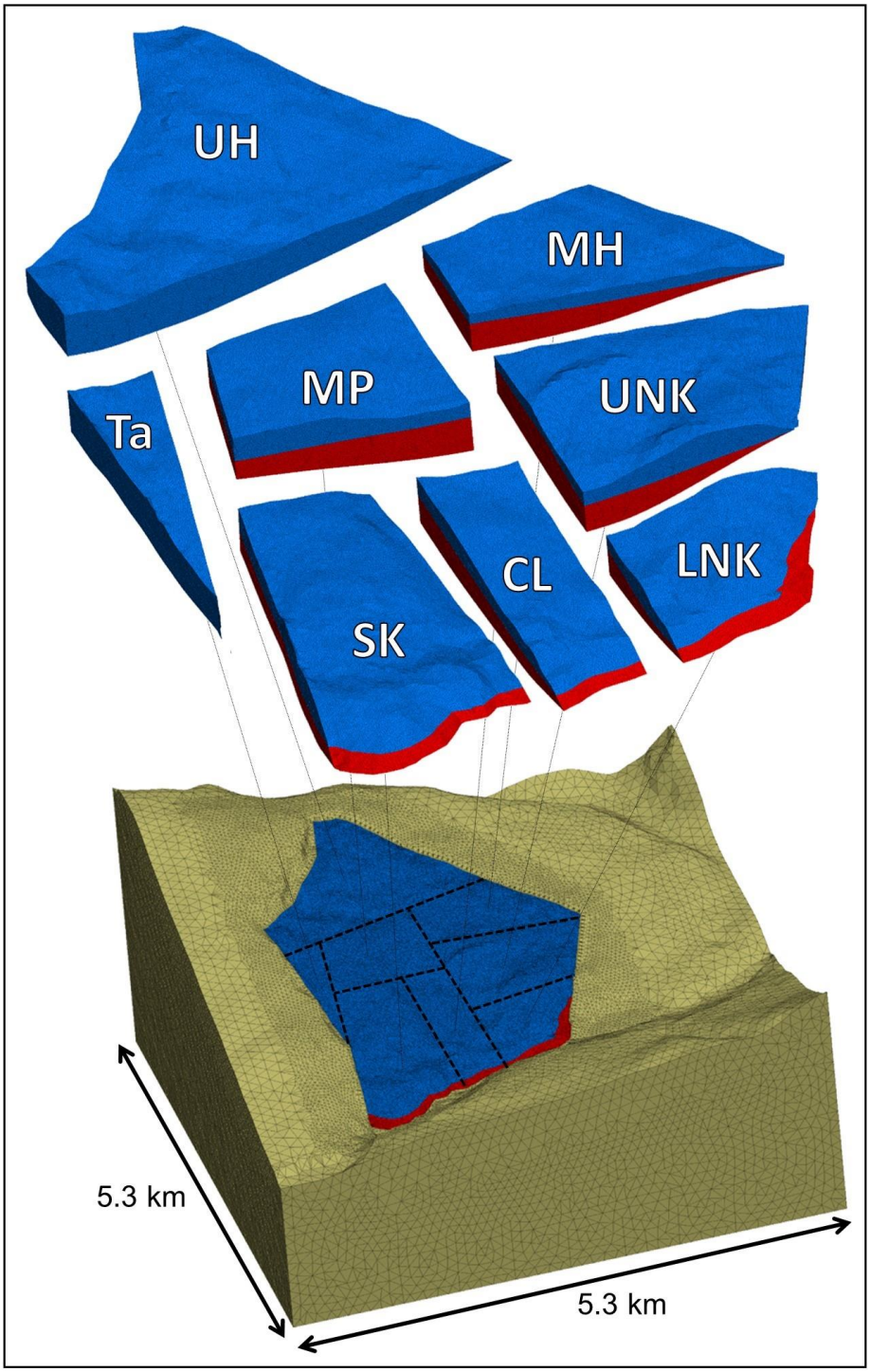

Figure 4 **Slope domains, based on Westin (2017), implemented in the three-dimensional 3DEC model of the Downie Slide. UH: Upper Hummocky Block; Ta: Talus Block; MP: Mid Plain Block; MH: Mid Hummocky Block; SK: South Knob Block; CL: Channelized Lower Block; UNK: Upper North Knob Block; LNK: Lower North Knob Block; b). The slide volume above and below the USZ is colored in blue and red, respectively. Note that only the LSZ is implemented in blocks UH and Ta, as they are considered as secondary failures in this model.**

Rock mass dilation has also been considered in the numerical model. It is known that the dilation angle decreases with the progressive deformation of the rock mass, and becomes null when the maximum volumetric strain is achieved. However, the definition of an appropriate dilation value for a large scale jointed/foliated rock mass for use in numerical models remains a challenging task. Based on empirical considerations, Hoek and Brown (1997) suggest that a preliminary value of $\phi/4$, $\phi/8$, and 0 may be used for good, average, and very poor quality rock masses, respectively. A more robust approach to evaluate rock mass dilation has been proposed by Alejano and Alonso (2005) that requires knowledge of the compressive strength, friction angle, and confinement conditions of the rock mass. In view of the large deformation that occurred at the Downie Slide, limited rock mass dilation may be expected, and a 2° dilation angle was assumed as a preliminary estimate for the rock mass. The shear strength parameters of the LSZ were based on previous direct shear testing (BC Hydro, 1974), which provided a friction angle ranging between 16° and 24°. Preliminary dry models in 3DEC, however, showed that no appreciable displacement would occur using these values. A back-analysis was therefore performed, allowing displacement to occur with a friction angle of 15°. Such behavior was expected in a dry model, as the absence of a water table would increase stability of the slope through increased effective stress along the sliding surface. Parameters assigned to the USZ were obtained by upscaling the LSZ strength parameters, in order to reproduce the lower displacement rates observed in the field slope monitoring data. Additionally, the LSZ beneath the blocks forming the upper portion of the Downie Slide (i.e., the upper hummocky region) was assigned higher strength properties due to the secondary nature of the failure mechanism. Table 1 and Table 2 summarize the mechanical parameters assigned to the geological materials and the discontinuities within the model, respectively.

Table 1 Summary of the deformable block properties used for the numerical investigation of the Downie Slide. Residual values are in brackets.

Property	Slide rock mass	Slope rock mass
Constitutive model	Strain-softening*	Elastic
Dry density (kg/m^3)	2,700	2,700
Saturated density (kg/m^3)	2,730	2,730
Bulk modulus (GPa)	1.8	1.8
Shear modulus (GPa)	0.9	0.9
Friction angle (°)	34 (30)	-
Cohesion (MPa)	2 (0.2)	-
Tensile strength (MPa)	0.4 (0.04)	-
Dilation (°)	2	-

*: Residual properties for strain-softening blocks are assigned after a strain of 0.02.

Table 2 **Summary of the shear surface and slide boundary properties used for the numerical investigation of the Downie Slide. Residual values are in brackets.**

Property	LSZ	USZ	LSZ - Secondary failure	Lateral and block boundaries
Constitutive model	Mohr-Coulomb	Mohr-Coulomb	Mohr-Coulomb	Mohr-Coulomb
Friction angle (°)	15 (12)	18 (15)	20 (18)	20 (18)
Cohesion (kPa)	100 (0)	200 (0)	200 (0)	0
Tensile strength (kPa)	20 (0)	40 (0)	40 (0)	0
Normal stiffness (MPa/m)	50	500	1,000	1,000
Shear stiffness (MPa/m)	25	250	100	100

In this numerical analysis it was decided, as assumed in Kalenchuk et al. (2012), not to explicitly include the joint sets within the block domains. This modelling approach provides several advantages, including: a) slope damage may form as a result of rock mass yielding (conversely, the implementation of joint sets would force slope damage to develop exclusively through dilation of fully-persistent joints, preventing yielding of intact material); b) a significant decrease in the model runtime is achieved (to as low as 10 days), potentially allowing limited parametric analysis to be conducted; c) allowing comparison of the numerical modelling results with previous three-dimensional analyses of the Downie Slide.

Three models were run, using different water table assumptions. Firstly, the model was run simulating a dry slope (Model 1). Then, two different models were run to investigate the effect of the piezometric head acting along the LSZ (Model 2a), and the USZ (Model 2b). Two water tables were constructed, using piezometric head data provided by BC Hydro. For the Model 2a, the hydraulic heads observed in the piezometers positioned at the depth of the LSZ were interpolated using a Kriging method and the software Surfer (Golden Software 2016). For the model 2b, the piezometers positioned at the depth of the USZ were used, instead (Figure 5). In order to separately investigate the effect of the pore pressures along the USZ and LSZ, plastic displacements were allowed to occur only along the shear zone for which the water table is implemented. In other words, in model 2a the USZ was assigned elastic properties, and sliding was only allowed along the LSZ. Conversely, in model 2b only sliding along the USZ was permitted, and the LSZ was assigned elastic properties.

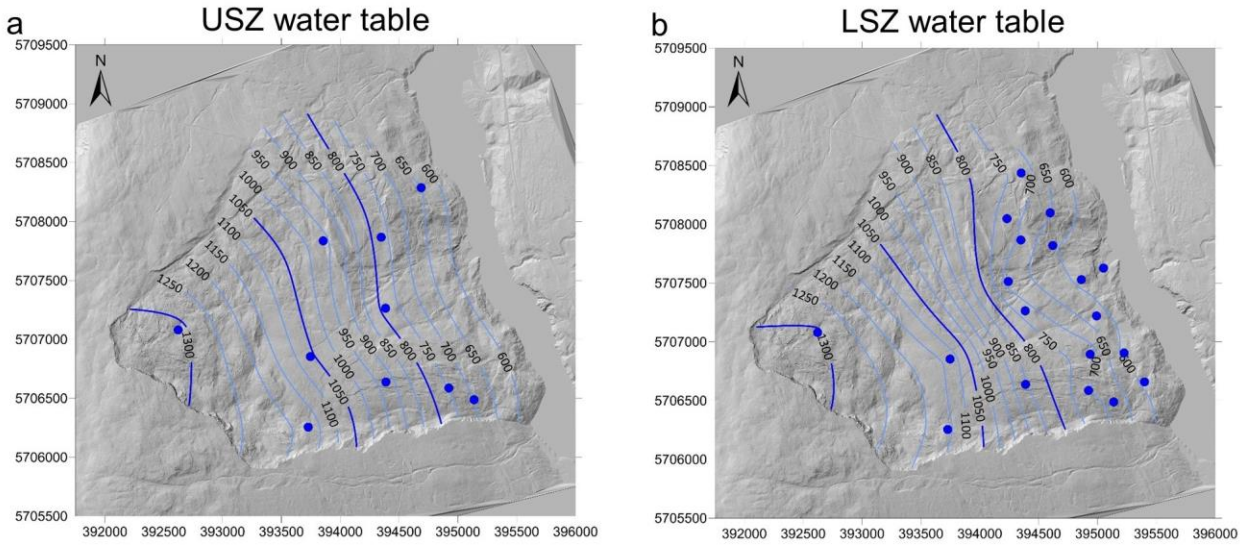

Figure 5 **Groundwater tables implemented in the numerical models, interpolated in Surfer. a: water table constructed using hydraulic heads observed along the LSZ (implemented in model 2a); b: water table constructed using hydraulic heads observed along the USZ (implemented in model 2b). Blue dots indicate the location of the piezometers considered for the Kriging interpolation of the water table.**

Throughout the numerical analysis, displacement data were recorded at virtual inclinometers implemented within the model. The location of the virtual borehole inclinometers coincided with installed borehole inclinometers at the Downie Slide. The virtual borehole inclinometers sampled displacement magnitude at every meter depth in both N-S and E-W directions, allowing displacement magnitudes to be computed during the post-processing.

In all simulations, a multi-stage model approach was used involving the following steps:

1. Geometry construction, domain subdivision, block zoning, and history point setup;
2. In wet models, implementation of water table, and initiation of pore pressure;
3. Elastic properties assigned to blocks and shear zones and the model then run to equilibrium;
4. Strain-softening constitutive criterion assigned to the rock mass blocks and the model then run to equilibrium;
5. High material properties assigned to the shear zones and the model then run to equilibrium;
6. Assumed material properties assigned to the shear zones, the model then run for 100,000 numerical time steps (200,000 for Model 2b), and the slope failure simulated.

Numerical models were run on a high-end workstation, with 6th generation Intel i7 3.2 GHz 8-core CPU and 128 GB RAM requiring on average, ten to twelve days to complete 100,000 numerical time steps. Results have been analyzed in 3DEC examining in particular displacement magnitude, failure state, and volumetric strain plots, which were found to provide useful information about simulated slope damage type and distribution. Volumetric strain ($\Delta V/V_0$) was employed to highlight areas of extension and compression, which were associated with compressive

and/or tensile damage accumulation. Monitoring data obtained from the virtual borehole inclinometers were exported and processed to derive cumulative displacement plots and displacement azimuths to allow comparison with observed slope monitoring data.

3.2. Description of the results

3.2.1. Model 1 – Dry slope

After 100,000 numerical time steps (cycles), maximum simulated displacement values of 7.5 m were observed in the northern section of the toe, with a gradual reduction in simulated displacement towards the western and southern scarps (Figure 6a). The upper portion of the Downie Slide shows the lowest simulated displacement, probably due to the low angle of the LSZ near the western cliff. The displacement of the slide is simulated with an azimuth of 70°N in the mid- and upper slope, which changes in the southern part of the lower slope to 90°N to 100°N. The direction of movement is controlled, in the numerical model, by the southern boundary of the slide area, which appears to kinematically constrain the movement of the central and upper slope blocks.

The analysis of the block plasticity failure state provided information on the failure mechanism in the discrete blocks forming the slide. Failed blocks are distributed between the lower and upper slope, whereas the mid slope remained largely intact, except along the southern boundary (Figure 6b). Tensile failure is predominant, and shear failure is concentrated in limited areas within the south knob and the upper hummocky blocks. Blocks that failed in tension appear to be grouped in north-south trending clusters in the north knob area. Tensile failure is also prominent in the south knob, where blocks failed in tension form clusters that strike in an east-west direction. The slope in this location is traversed by an area of predominantly north-south trending shear failure.

The volumetric strain plot shows positive strain (i.e., dilation) in the upper portion of the slope (upper hummocky block), as well as within the northern and southern slide blocks (south knob, upper and lower north knob blocks) (Figure 6c). Groups of zones with relatively high volumetric strain ($\varepsilon_v > 2.5e\text{-}3$) are organized in linear features, which extend in a north-south direction in the northern portion of the slide. More limited, southwest-northeast features are simulated along the northern boundary of the slide area. Along the southern boundary of the slide, east-west extensional features developed during the simulation. A complex network of extensional features also developed at the toe of the slide, in the northern part of the southern damage domain. Here, north-south features overprint east-west striking features. North-south striking dilational features also developed within the upper damage domain. Negative volumetric strain (i.e., compression) was locally observed in the central part of the northern damage domain, and at the toe of the south knob block. Positive volumetric strain was found to continue with depth, indicating that both external and internal damage exist in the areas where surface dilation was observed (Figure 6d-f). Negative volumetric strain (e.g., compression) was observed along the LSZ, where the gradient of the shear zone decreases, and may be associated with the development of a transition zone at the interface between the active and passive blocks of the slide (Figure 6d).

The volumetric strain plot was imported as a raster file in ArcGIS (ESRI, 2017). Here, lineaments simulated in the analysis were mapped, their average trend computed and plotted on rosette diagrams using DIPS (Rocscience, 2019). A preferential NNW-SSE lineament orientation was noted throughout the slide blocks, while intense NE-SW features were simulated in the south knob and north knob slide blocks (Figure 5g).

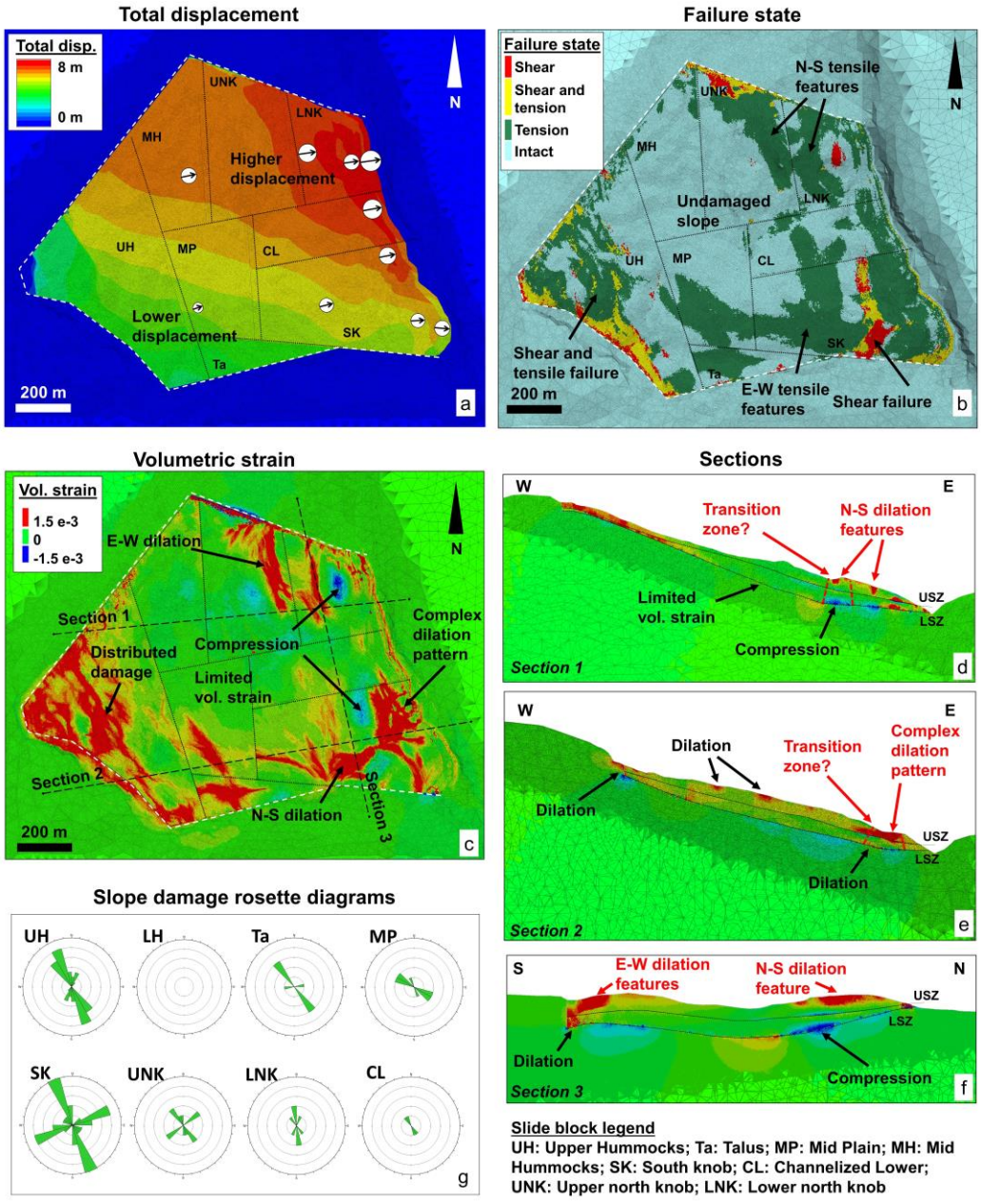

Figure 6 **Results of the numerical analysis of Model 1 (dry slope) at 100,000 numerical time steps. a: total displacement plot. Arrows indicate the modelled displacement azimuth; b: block failure state plot; c: volumetric strain plot. Red and blue indicate increase and decrease in volume, respectively (extension and compression); d,e: sections east-west through Downie Slide showing the simulated volumetric strain; f: section north-south through Downie Slide showing the simulated volumetric strain; g: rosette diagrams showing the preferential slope damage feature orientation within the slide blocks.**

3.2.2. Model 2a – Water table above the Lower Shear Zone

Model 2a simulates the slide displacement along the LSZ, and includes the pore pressures acting along the lower sliding surface. A saturated density of 2,730 kg/m^3 was assigned to the material below the water table. An additional, hydrostatic load was also applied to the slope below 573 m, to account for presence of the reservoir. Throughout the Model 2a simulation, an elastic constitutive criterion was assigned to the USZ in order to prevent sliding.

The simulation required 12 days, and was terminated after 100,000 numerical time steps (cycles), when a maximum displacement of around 12 m was observed. The greatest displacement magnitude was observed in the northern part of the lower slope. Simulated displacements decrease towards the western and southern scarps (Figure 7a). Sliding predominantly occurs in a northeast direction (azimuth 70° N), whereas toward the southern boundary displacements follow an eastward trend (90-95° N).

The plasticity zone failure state plot indicates that tensile failure occurred throughout the lower slope, whereas shear failure is limited to the south knob and the upper and lower north knob blocks. Mixed tension and shear failure affected the upper portion of the slope (Figure 7b). In the central portion of the slope blocks were subjected to low volumetric strain and showed limited failure throughout the numerical simulation.

The volumetric strain plot for Model 2a shows strong similarities to Model 1. North-south and northeast-southwest trending extensional features developed in the northern portion of the slope (Figure 7c-d). A complex network of damage features was simulated at the base of the south knob (Figure 7e). Positive volumetric strain is distributed throughout the upper slope, where no clear damage accumulation pattern can be observed. In the southern portion, east-west features were simulated, which continue with depth reaching the LSZ (Figure 7f).

The lineaments modelled in the analysis were approximately mapped and plotted on rosette diagrams. Modelled lineaments predominantly strike in a NNW-SSE direction. Slope damage features striking in a southwest-southeast direction were also modelled within the south and north knob slide blocks (Figure 7g).

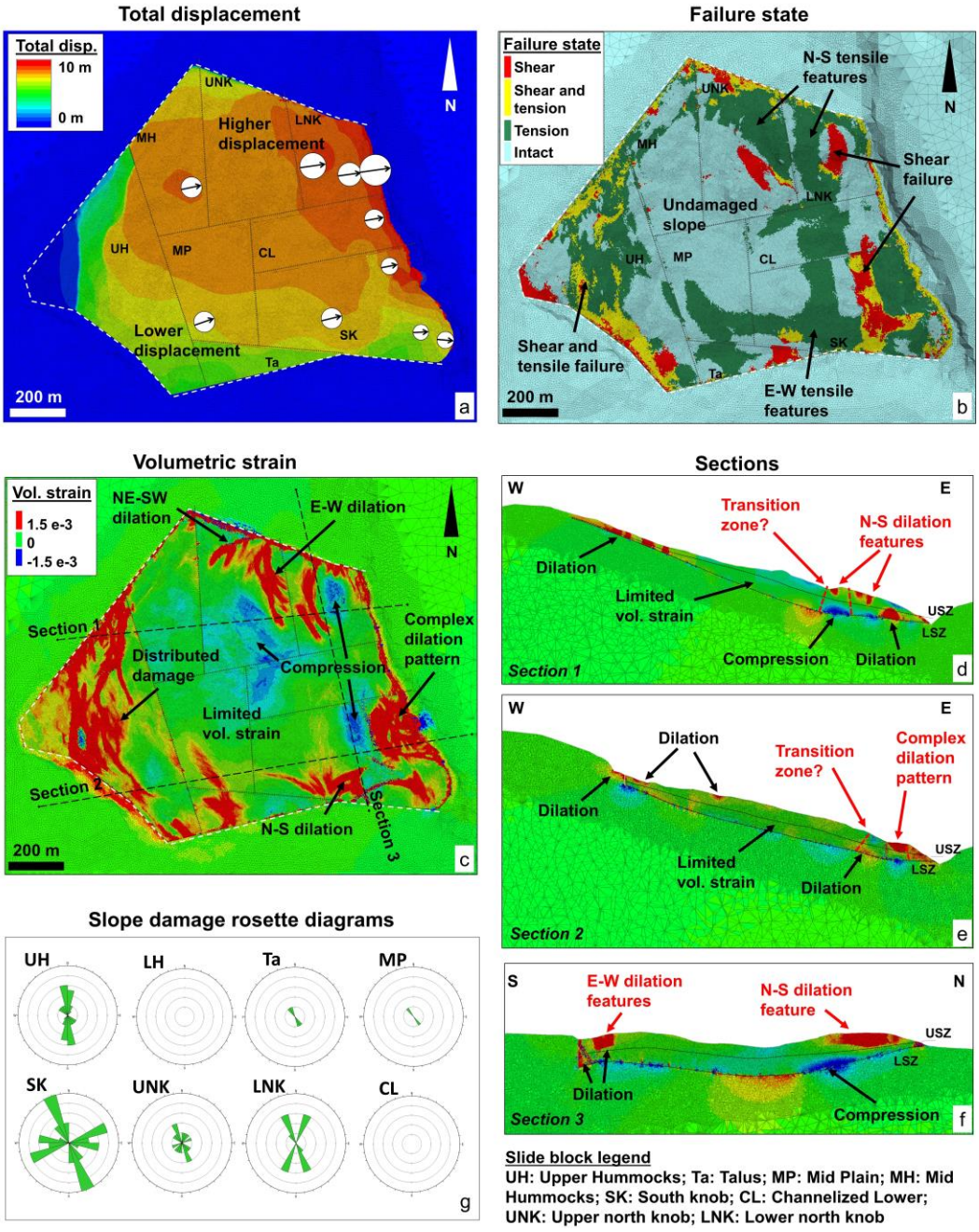

Figure 7 **Results of the numerical analysis of Model 2a (water table above the LSZ) at 100,000 numerical time steps. Note the similarity with Model 1. a: total displacement plot. Arrows indicate the modelled displacement azimuth; b: block failure state plot; c: volumetric strain plot. Red and blue indicate increase and decrease in volume, respectively (extension and compression); d,e: sections east-west through Downie Slide showing the simulated volumetric strain; f: section north-south through Downie Slide showing the simulated volumetric strain; g: rosette diagrams showing the preferential slope damage feature orientation within the slide blocks.**

3.2.3. Model 2b – Water table above the Upper Shear Zone

Model 2b analyzes the effects of the displacement along the USZ, considering the pore pressure that exists above the upper sliding surface. A saturated density of 2,730 kg/m^3 was assigned to the material below the water table. The water mass forming the reservoir was also accounted for by applying an additional load below 573 m a.s.l.

A maximum displacement of about 1 m was obtained after 200,000 numerical time steps (cycles). The largest displacements occurred in the southern portion of the slide, between the channelized lower and the south knob blocks (Figure 8a). Displacement magnitude decreased towards the north and west. The predominant displacement azimuth is approximately 75° N, except for in the southern portion of the south knob block where the direction of movement sharply changes to 100° N, causing a single, linear, extensional feature to form parallel to the southern scarp (Figure 8c). Small areas of positive volumetric strain are limited to the toe of the slide, with no significant deformation simulated elsewhere in the slide area.

The block failure state plot shows limited tensile failure in the lower slope, mostly concentrated in the southern and central portions of the slide (Figure 8b). Shear failure can be observed in the upper slope, particularly along the western headscarp.

The low level of slope damage is also highlighted by the slope damage rosette plots, which show that damage features, striking in an east-west direction, were only modelled in the south knob slide block (Figure 8g).

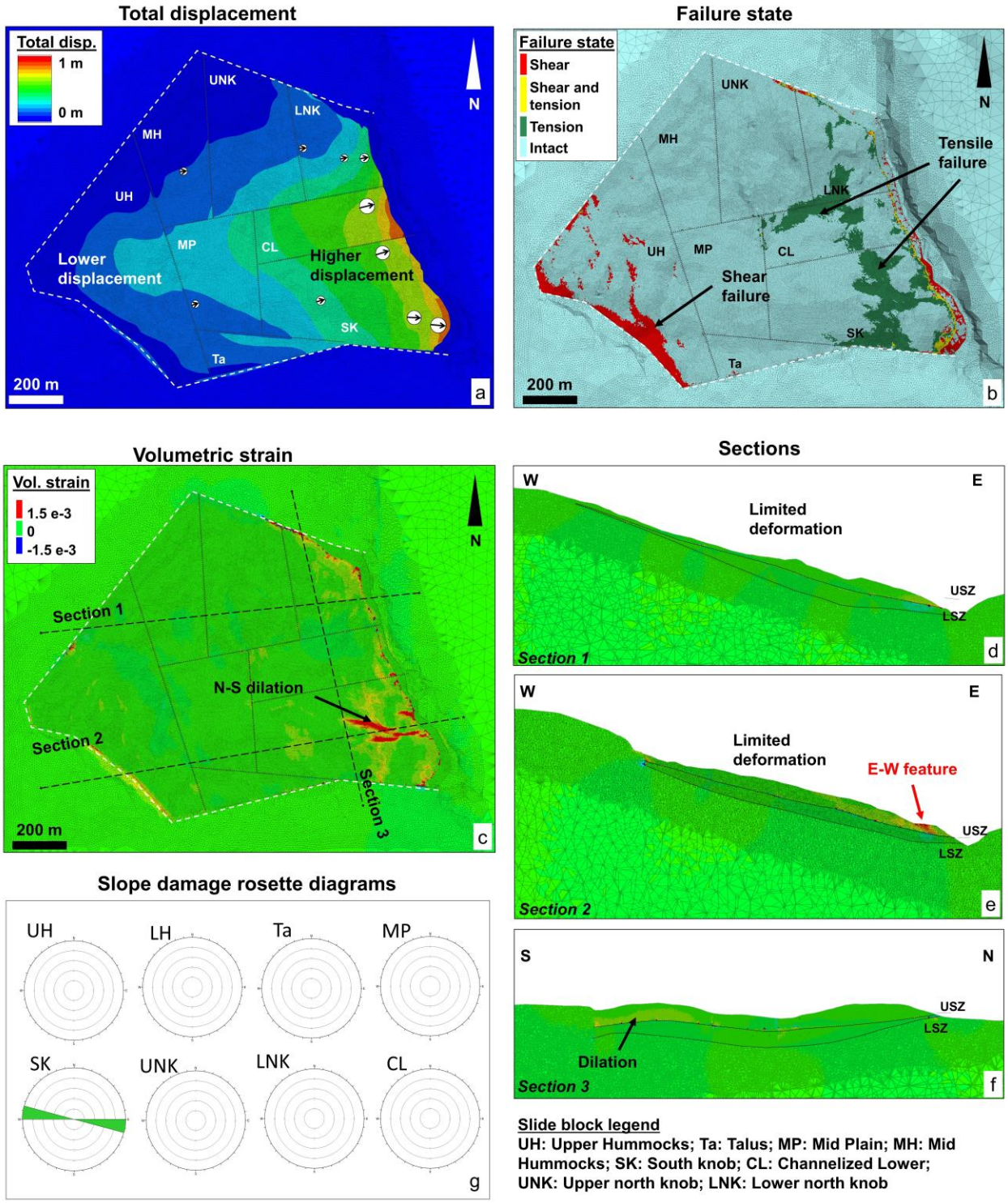

Figure 8 **Results of the numerical analysis of Model 2b (water table above the USZ) at 200,000 numerical time steps. a: total displacement plot. Arrows indicate the modelled displacement azimuth; b: block failure state plot; c: volumetric strain plot. Red and blue indicate increase and decrease in volume, respectively (extension and compression); d,e: sections east-west through Downie Slide showing the simulated volumetric strain; f: section north-south through Downie Slide showing the simulated volumetric strain; g: rosette diagrams showing the preferential slope damage feature orientation within the slide blocks.**

4 Discussion

4.1. Comparison with slope damage domains

Numerical modelling of the Downie Slide assuming a plastic, strain-softening constitutive criterion has allowed slope damage to be progressively simulated throughout the analysis. A validation of the numerical results has been undertaken by visually comparing the volumetric strain and failure state plots with the slope damage domains identified in the ALS hillshade map (Figure 9, Figure 10, Figure 11). The 3DEC damage modelling results compare well with the observed external slope damage in the ALS dataset. The virtual inclinometer plots (i.e., the displacement directions) were also compared with real monitoring datasets (Figure 12).

A good agreement was observed between the ALS maps and the results of Model 1 and Model 2a. The north-south and northeast-southwest focused tensile features observed in the volumetric strain plot are similar to the external slope damage features mapped in the ALS along the northern damage domain (Figure 9). Compared to the observed slope damage, simulated damage within the slope appears to be more curved and less linear. The inclusion of rock mass jointing would provide additional constraint on the orientation of the extensional features but would require an impractical increase in computational requirements and time. In the southern part of the slide area, east-west trending extensional features simulated in the models are consistent with the slope damage orientation observed in the southern damage domain on the ALS map (Figure 10). The accumulation of shear damage along the southern boundary, as observed in the failure state plots, appears to agree well with the presence of the counterscarps recognized in the ALS dataset. The central part of the lower slope, the most active area of the Downie Slide, shows a slight compression (i.e., negative volumetric strain values) in Model 1 and Model 2a. This result is expected, as the area is located at the intersection between the southeast- and northeast-dipping portions of the lower shear zone. All the model simulations indicate that the central part of the Downie Slide remained substantially undamaged and undeformed throughout the simulation, in good agreement with the external slope damage observed in the ALS (Figure 2a). This lack of slope damage is likely due to the uniform dip of the LSZ, which allows the unstable mass to slide without significant internal deformation. Distributed, tensile and shear damage is simulated in the upper slope in Model 1 and Model 2a, which appears to agree well with the damage and hummocky surface observed both in the ALS and in the field (Figure 11). It is interesting to note that both Model 1 and 2a display relatively high absolute values of volumetric strain along both the LSZ and the USZ, suggesting that a significant accumulation of internal slope damage can be simulated for displacements as low as 8-10 m. This area of increased internal slope damage appears to agree with the observed increase in thickness of the USZ and LSZ, suggesting that the progressive slide displacement (estimated at about 300 m) was an important factor in the shear zone thickening process.

Results of Model 2b indicated the simulation of east-west extensional features at the base of the south knob block (Figure 10). Although these features cannot be readily compared with any lineament visible in the ALS, its

orientation and location are consistent with a north-south extension that is apparent throughout the southern portion of the slide in Models 1 and 2a.

Model 1 (which includes both LSZ and USZ) and Model 2a (LSZ only) were capable of reproducing the spatial distribution of slope damage observed in the ALS, as well as the mode of failure of the material (e.g., shear vs. tensile). Conversely, Model 2b (which included the USZ only) does not reproduce the damage features recognized in the ALS.

Numerical modelling appears to indicate that the lower shear zone played a critical role in formation of the damage that is observed in the field. The role of the upper shear zone appears more limited, however further analyses should be undertaken to investigate in detail its effects on the evolution of surficial or localized external slope deformations.

From a comparison with the observed slope damage features, modelled slide activity on the USZ is not considered to have created the larger scale slope damage, which is attributed to significant slide displacement activity on the LSZ, but contributed to complementary slope damage effects. These model observations collectively suggest that the initial and significant slide displacement activity occurred on the LSZ, while the USZ developed during the evolution of the slide, and has now become a significant contributor to the present day slide mechanism.

A comparison of the virtual borehole inclinometer records with the slope monitoring data was also undertaken (Figure 12). As an example, Figure 12b shows the comparison between the monitoring log from the inclinometer S51, and its virtual counterpart, obtained from Model 1. Deformation occurring along the lower shear zone in the east and north directions were plotted to investigate the direction of displacements. The resulting virtual displacement vectors were then compared with the directions of displacement calculated for the real inclinometers (see table inset in Figure 12a). The virtual inclinometer results for both Model 1 and Model 2a are characterized by a more a uniform distribution in azimuth compared to the real monitoring data, with the largest differences observed in inclinometers at the base and in the northern part of the slope (Figure 12a). No appreciable difference was observed between the displacement direction in Model 1 and Model 2a. Factors that may affect the comparison of simulation with borehole inclinometer records include the quality of the field monitoring data and the material properties assigned to the blocks in the model. Data quality may be limited for the older borehole inclinometers, installed in the 1980s, which are mainly located in the lower slope. Experience gained through the analysis of similar instruments at other BC Hydro sites suggests that uncertainties in the displacement direction may be in the order of ±20°, due to outdated installation techniques and potential deformations of the casing. The material properties assigned to the blocks within the 3DEC model may also affect the direction of movement. Numerical modelling has been conducted using a single set of mechanical rock mass properties, ignoring the type and varying amount of damage already present within the various blocks. Correcting the mechanical parameters to include the slope damage mapped in the ALS may affect the ongoing deformation behavior of the blocks, allowing for displacement azimuths to be obtained with increased confidence. It should also be stressed that the variations in the shear surface dip and dip direction are dependent upon the distribution of the borehole and their spacing; it is to be expected that localized errors in the

517 interpolation of the shear surface topography will inevitably be present that would influence any comparison between
518 simulated and observed displacement. Notwithstanding such uncertainties, the comparison between simulated
519 displacements and observed borehole inclinometers logs shows remarkable agreement given the necessary data
520 assumptions used in this study.

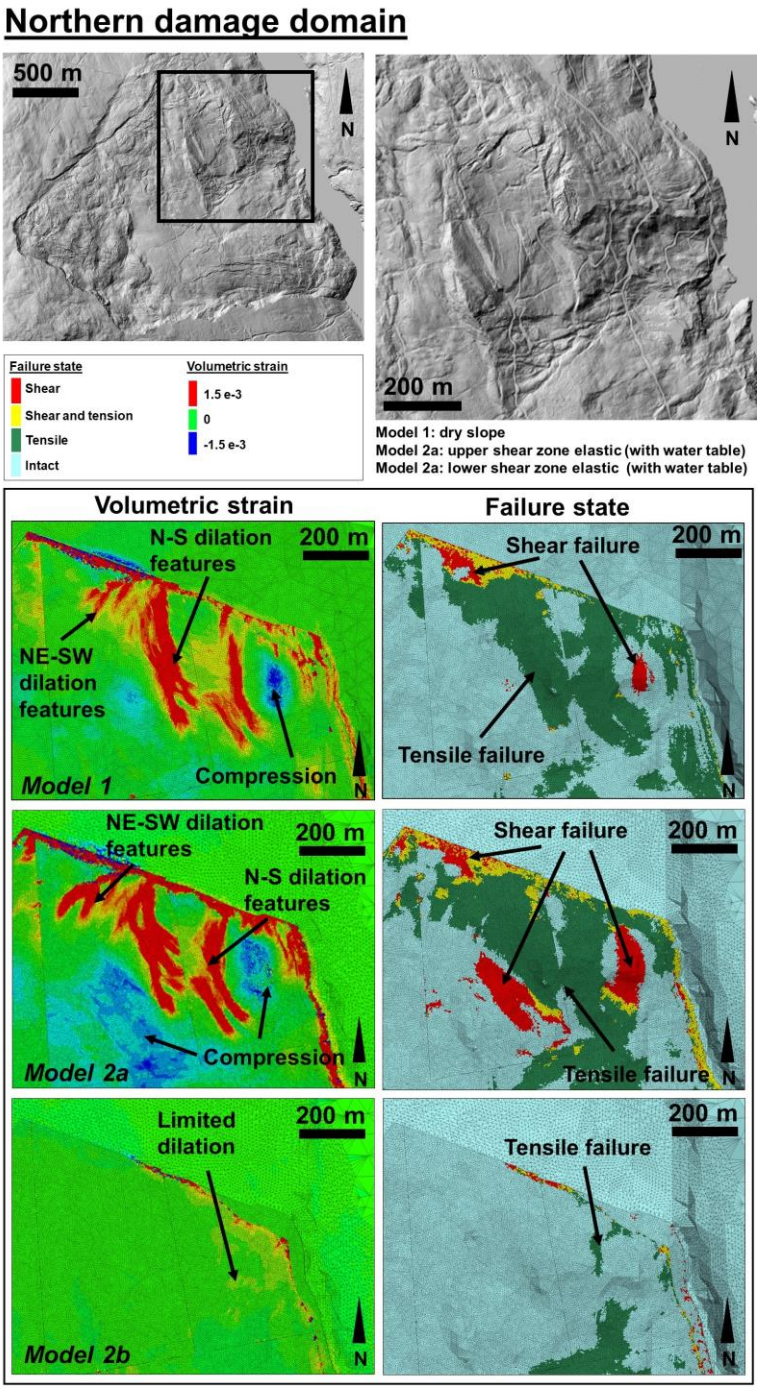

Figure 9 **Northern damage domain: damage comparison between the volumetric strain and zone failure state 3DEC plots at 100,000 numerical time steps (200,000 for Model 2b) and the ALS hillshade map. Focused tensile damage developed in Models 1 and 2a. North-south oriented features in the volumetric strain plot correlate closely with slope damage and deformations observed in the ALS. Failure state plots show predominantly tensile damage throughout the domain. Model 2b shows limited deformation and failed zones.**

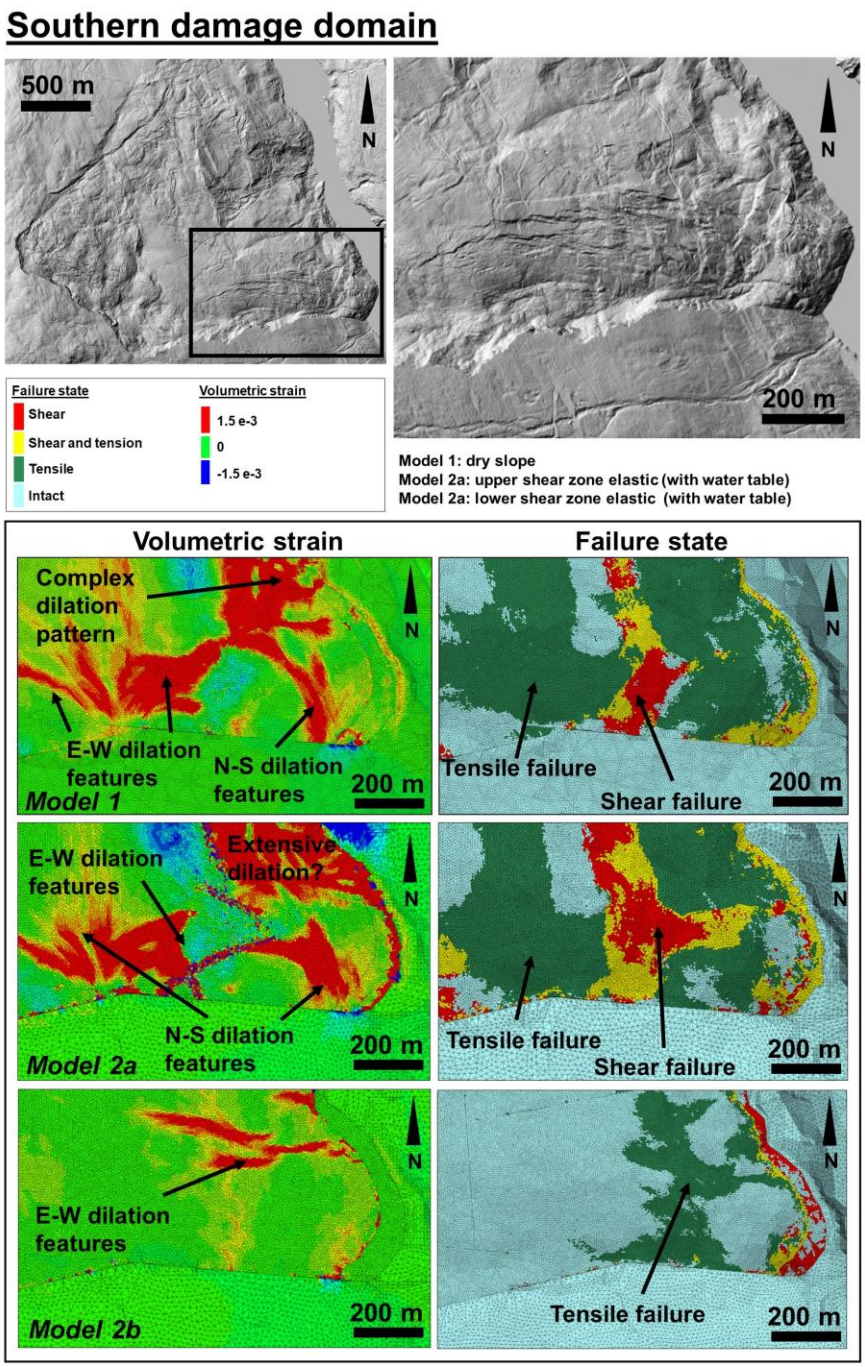

Figure 10 **Southern damage domain: damage comparison between the volumetric strain and zone failure state 3DEC plots at 100,000 numerical time steps (200,000 for Model 2b) and the ALS hillshade map. Focused tensile damage developed in Models 1 and 2a. East-west oriented features, resulting from a north-south extensional behavior of the slope, agree with slope damage mapped in the ALS. Failure state plots show predominantly tensile damage throughout the domain, with shear failure in proximity of the base of the slope. The location of zones failed in shear is similar to the counterscarp recognized in the ALS. Model 2b shows the simulation of a dominantly east-west trending feature that results from north-south extension.**

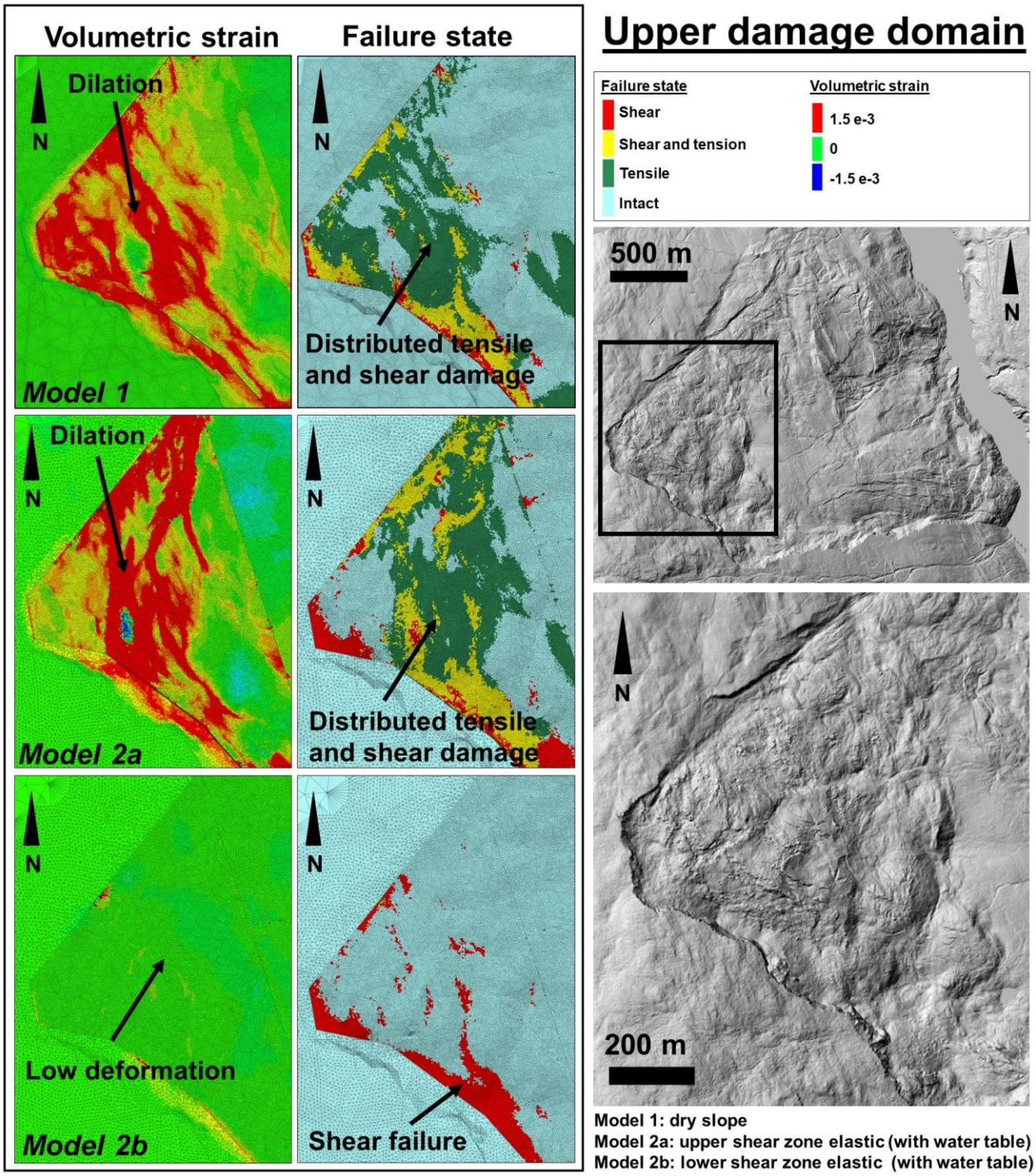

Figure 11 **Upper damage domain: damage comparison between the volumetric strain and zone failure state 3DEC plots at 100,000 numerical time steps (200,000 for Model 2b) and the ALS hillshade map. Distributed slope damage in the form of volumetric strain and failed zones can be observed in Models 1 and 2a. Model 2b showed only limited deformation and failure.**

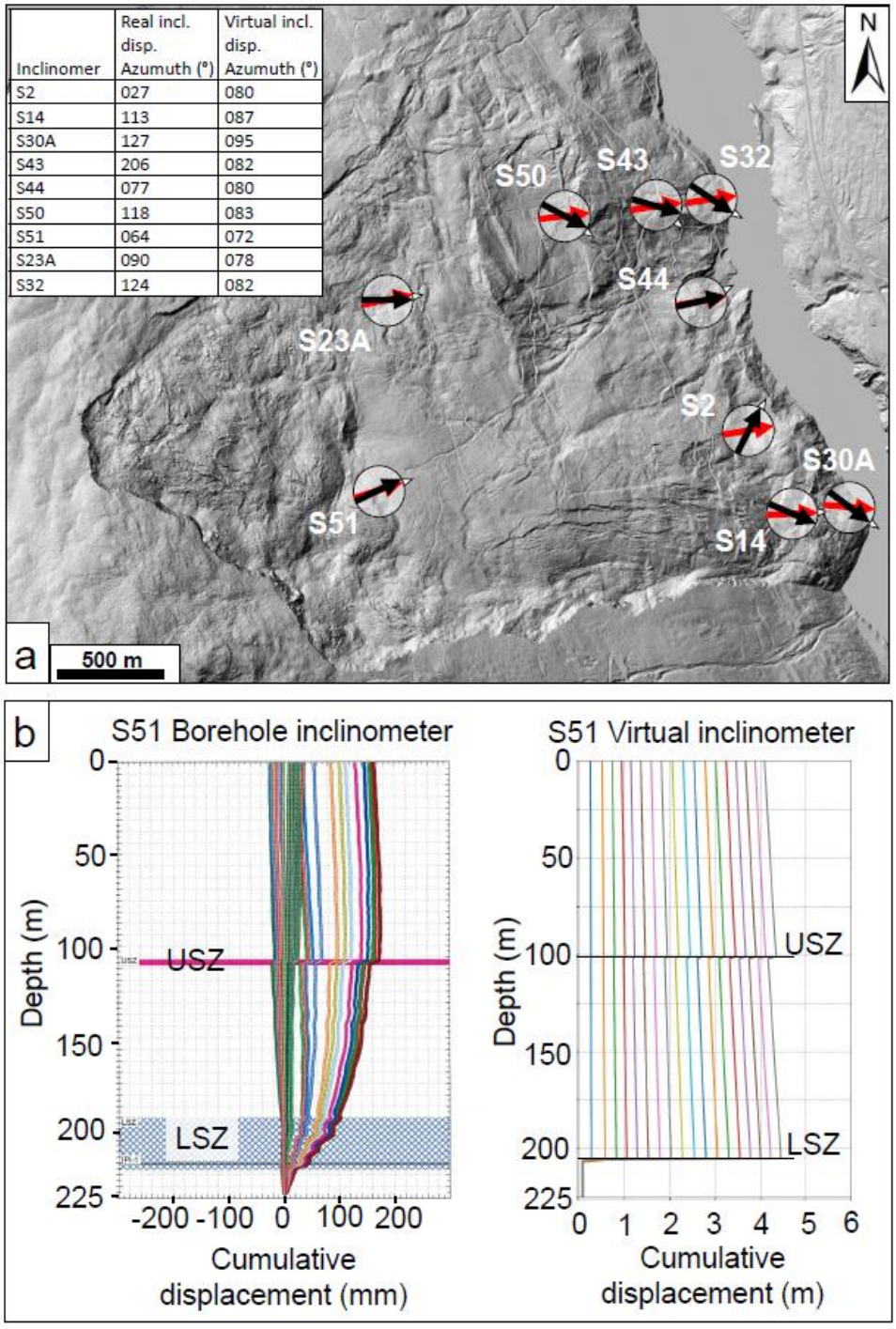

Figure 12 **Comparison of displacement direction of real and virtual borehole inclinometers along the LSZ at 100,000 numerical time steps. a: circles show the location of the investigated boreholes. White arrowheads show the dip direction of the LSZ at the borehole location. Black and red arrows show the displacement azimuth of real and virtual inclinometer, respectively. The table shows the azimuth values computed from the recorded and simulated inclinometer plots. As no significant differences were observed between displacement direction in Model 1 and Model 2a, the virtual displacement azimuth are representative of both models; b: example of real and virtual borehole inclinometer logs (S51 inclinometer monitoring log, provided by BC Hydro, is presented as an example).**

The volumetric strain plot for Model 1 was qualitatively compared with the lineament intensity analysis presented in Westin (2017). In that work, each of the twelve domains was assigned a L_{21} value, computed as the total length of the lineaments mapped in the domain divided by the surface area of the domain, thus providing a preliminary quantification of the external slope damage intensity. In particular, high lineament intensities were observed within the south knob area, in the north knob area, and in the upper slope. High lineament intensity was also observed in the northern part of the central slope. A good agreement exists between the lineament intensity map of Westin (2017) and the volumetric strain plot with positive volumetric strain increments simulated in the upper part of the slope, in the northern domain, and in the southern domain (Figure 13).

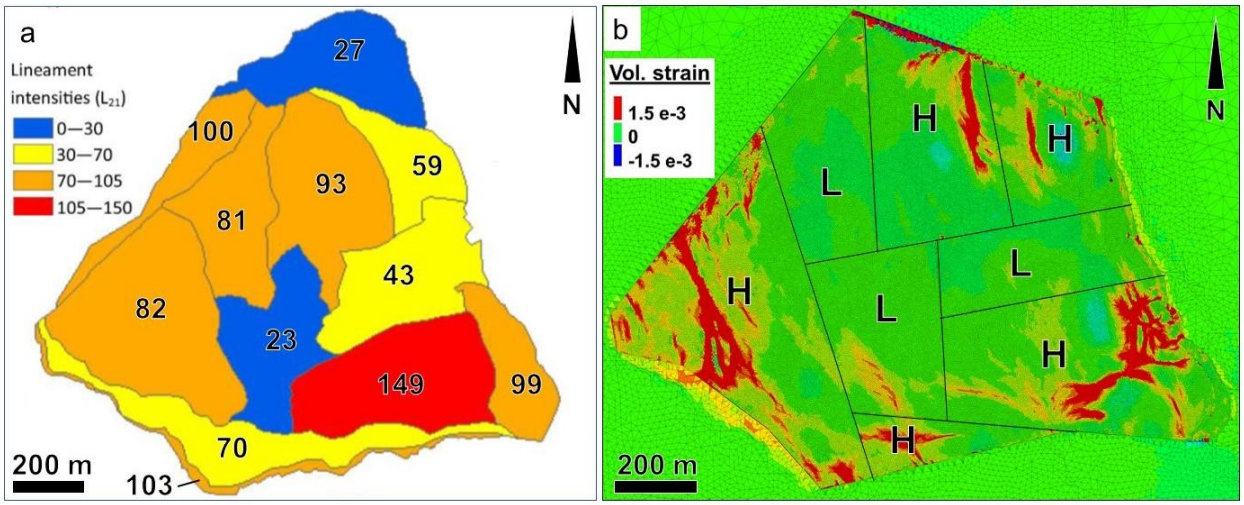

Figure 13 **Comparison between the lineament intensity map (a, modified from Westin, 2017), and the 3DEC volumetric strain plot from Model 1 (b). In the lineament intensity map, the numbers show the lineament intensity (x 10^{-4}) for each domain. In the volumetric strain plot, L and H qualitatively indicate low and high relative external slope damage, respectively.**

4.2. Comparison with previous numerical modelling of the Downie Slide

Previous investigations conducted at the Downie Slide, described in published and unpublished reports and papers largely focussed on four main aspects: the structural and regional setting of the area where the Downie Slide formed, the mechanisms underlying the initiation of the instability, the geomorphic characterization of the landslide area and the role of the assumed sliding surface morphology on surface displacement distribution. Kjelland (2004) investigated the initiation of the failure using the finite difference software FLAC 4 (Itasca Consulting Group 2000). He modelled the gradual retreat of the glacier from the Columbia River Valley, and the resulting slope failure at the Downie Slide due to debuttressing and kinematic release. He observed a good agreement between the numerical results and the displacement distribution at depth in the slope using a strain-softening, ubiquitous joint constitutive model. Kalenchuk et al. (2012) employed the three-dimensional distinct element software 3DEC (Itasca Consulting Group 2016a) to investigate the effect of the shear zone thickness over the displacement rates, comparing the displacement distribution of the numerical results with the slope monitoring data. The shear zone was modelled as a

joint with variable stiffness values throughout the slide area. High shear zone thickness was associated with lower shear and normal stiffness values. A good agreement was observed between simulated and measured displacement rates, and the importance of secondary shear zones within the slide area was highlighted. Subsequently, the influence of changes in the water table level (e.g., rapid reservoir drawdown, loss in drainage capacity) on the deformation rates of the Downie Slide was investigated (Kalenchuk et al. 2013b).

Compared to previous studies, we employ a 3D DEM, strain-softening numerical model to investigate in detail the correlation between displacement distribution, basal sliding surface morphology, ground water, and slope damage. The effectiveness of the numerical model to reproduce the slope damage features observed on the ALS dataset is demonstrated, suggesting that, if certain conditions are met (e.g., presence of a complex sliding surface), surface features can be used to constrain and validate numerical modelling results. Additionally, the capability of virtual borehole inclinometers to register not only the displacement magnitude, but also the displacement direction with depth (i.e., when displacement magnitude is monitored in mutually orthogonal directions) has also been highlighted, allowing for improved comparison and correlation between in-situ monitoring systems and numerical models.

4.3. Comparison with other slowly moving rockslides

Slowly and extremely slowly moving rockslides often involve the displacement of material along foliation and schistosity. These slope instabilities in some cases may involve significant volumes of rock mass, and assessing the mechanisms underlying the deformation is of primary importance for the safeguard of nearby communities and infrastructure. It has been observed that slowly moving landslides may display periods of increased velocity, but are generally unlikely to evolve into fast movements without external disturbances (Bonzanigo et al., 2007; Zangler et al., 2010; Glastonbury and Fell, 2008). However, in view of the very large volumes of rock mass involved, the understanding of the mechanisms controlling their behavior and displacement, together with the monitoring of the displacements, is critical to ensure a timely response in case of an evolution in displacement style and rate. In general, these large slope instabilities share some important characteristics:

- *Geotechnical and lithological characteristics.* They generally develop in crystalline rocks that are characterized by pervasive foliation or schistosity. As a result, a creeping behavior may develop within the slide material, which becomes increasingly evident in the long-term. In the short term, deformations remain predominantly concentrated along sliding surfaces and shear zones;

- *Multi-block structure*. They are generally constituted by multiple blocks formed as a result of the slope deformation (such as internal shears), or divided by inherited geological structures. The complex, multi-block structure can enhance the kinematic freedom of the entire slide body and the single blocks, and therefore it plays a critical role in controlling displacement distribution;

- *Sliding surface characteristics*. They often displace along one or more sliding surfaces with complex morphology, as a function of the structural setting where the slide develops. In some cases, movements can be observed between the blocks forming the slide body;

- *Landslide stage*. From a geotechnical perspective, sliding surface(s) are often in a condition of residual strength, which limits the likelihood of sudden displacement accelerations. This often indicates that the landslide is in a post-failure or reactivation stage;

- *Hydrogeology*. They are typically characterized by a complex hydrogeological setting, with multiple independent aquifers sometimes with artesian conditions. Distribution of ground-water pressure along the sliding surface(s) often controls the displacement rates.

- *Geomorphology*. They generally develop in slopes that are over-steepened at the toe, due to river or glacial erosion. The remaining part of the slide area can be characterized by gentler slopes.

Many examples of very and extremely slowly moving deep-seated rockslide have been described in literature. Table 3 list some of the most significant: for each site, the geological factors controlling the displacements, and similarities with the Downie Slide are presented.

Table 3 Summaryof the geological characteristics of selected very and extremely slowly moving rockslides described in literature, and observed similarities with the Downie Slide.

Landslide	Description	Similarities with the Downie Slide	References
Dutchman Ridge Slide (British Columbia, Canada)	Translational, first time slide (volume = 115 x 10^6 m^3, max thickness = 110 m) on the W shore of the Mica Lake. Slide is composed of mica-schist, mica-gneiss, quartz-gneiss, and marble, with foliation dipping into the slope. Displacement (up to 20 mm/y) started with reservoir impoundment along a fault dipping 29° downslope. Drainage adit and drainholes were installed to slow down the moving mass (down to 1-2 mm/y).	Similar lithology, but with different foliation orientation; displacement driven by ground water pressure in compartmentalized aquifers.	Moore, 1993
Campo Vallemaggia landslide (Switzerland)	Massive translational rockslide (volume = 0.8 x 10^9 m^3, max thickness = 300 m). Slide body is formed by amphibolites, micaceous schist, gneiss. Slope oversteepening due to river erosion initiated deep-seated displacement, along down-slope dipping foliation. Monitoring system shows variable displacement rates with intermittent increases, 1-2 cm/y, up to 3-4 m/y. A drainage adit was excavated below the sliding surface to increase stability.	Similar size and geomorphic characters; complex hydrogeological setting, including artesian aquifers, driving slope displacement; slide body subdivided in multiple independent blocks	Bonzanigo et al., 2007 Eberhardt et al., 2007
Aknes Slide (Norway)	Translational rockslide (volume = 35-40 x 10^6 m^3, max thickness = 65-70 m) on the shore of the Geirangerfjord. Slide is composed of quartz-dioritic to granitic gneiss, with foliation sub-parallel to the slope, heavily folded at the headscarp. Observed surface displacement rates averaging 3-4 cm/y. Displacement direction is partially controlled by a crevice that provides lateral release.	Displacement along slope-parallel foliation; slide composed of 4 partially overlapping blocks displacing at different rates and directions.	Ganerod et al., 2008

Nine Mile creek landslide (New Zealand)	Massive compound rockslide (volume = > 1 x 10^9 m^3, max thickness = 260 m) on the E shore of the Clyde Dam reservoir. Slide is constituted by schists, with foliation dipping sub-parallel to the slope. Measured surface displacement rates up to 2 mm/y.	Similar size and geomorphic characters; displacement along slope-parallel foliation; compartmentalized aquifers within the slide body, sometimes in artesian conditions	O'Brein et al., 2016 Macfarlane, 2009
Hochmais–Atemkopf rockslide system (Austria)	Cluster of nested translational rockslides along the shore of the Gepatsch reservoir (total volume = 290 x 10^6 m^3, max thickness = 220 m). Slide is composed of paragneiss, mica schist, and orthogneiss, with foliation dipping into the slope. Displacements occur along discontinuities normal to foliation. Ground surface displacement rates are up to 2.5 cm/y.	Complex, multi-block landslide structure; structurally-controlled sliding surface	Zangler et al., 2010

5 Conclusions and future work

Lithology, geological structures, and the geomorphic evolution of the valleys are all important factors that influenced, and continue to influence, the kinematic configuration of the slope, and in turn the nature, distribution, and orientation of the slope damage developed at the Downie Slide. The investigation of slope damage from ALS, boreholes, and remote sensing can provide important insights on the spatial variations in slope deformation.

In this study, 3D numerical modelling of the Downie Slide was undertaken to investigate the role of shear zone morphology and groundwater on the characteristics of external slope damage observed in the ALS dataset. Simulation results showed that the complex geometry of the lower shear zone has a strong control on style and spatial distribution of external slope damage at the Downie Slide. Conversely, the geometry of the upper shear zone has limited influence on the evolution of slope damage. Additional investigations should focus on the role of the USZ on the evolution of local, smaller scale instabilities. Future analyses should also explore the effects of the pre-existing slope damage on the displacements within the slide. Specifically, initial material properties for each block should be down-scaled proportionally to the amount of damage observed in the ALS dataset. The quality in the reconstruction of the lower and upper shear zones is directly related to the borehole density across the slide area. Therefore, the collection of additional subsurface data in areas sparsely instrumented, including the boundaries and the upper part of the slope, may be beneficial in further constraining the shear zone geometry and improve the reliability of the numerical modelling results.

Numerical modelling results indicate that the principal effect of pore water pressure along the shear zones is on the magnitude of the simulated displacement. However, a simplified approach was used in this preliminary study, which involved the analysis of the water pressure acting on the lower and upper shear zones in two distinct models.

In order to include both shear zones in a single model, the variations in pore pressure within the slope should be known a priori, due to the complexity of the hydrogeological system at the site. Therefore, a detailed three-dimensional hydrogeological model would be required to assess the pore pressure distribution throughout the slope before incorporation into three-dimensional geomechanical models. This approach would allow a more comprehensive validation of critical pressures levels, and the assessment of their variations. Additionally, the effects of slope damage formation and accumulation on the permeability of the rock mass should be addressed. An increased porosity may facilitate the migration and redistribution of pore water pressure within the slope, with potential controls on the displacement rates of the slide.

This paper highlights an innovative method of comparing observed and simulated slope damage features using ALS – GIS analysis and 3DEC modelling respectively. The orientation, type, and distribution of ALS slope damage features has been shown to be a valuable method of validating and constraining the 3DEC numerical modelling results, particularly when used in combination with subsurface borehole inclinometers and GIS characterisation of the sliding surface geometry. The authors suggest that detailed characterization of slope damage using remote sensing, if possible combined with change detection and/or InSAR, should be considered a fundamental part of site investigation and monitoring of major landslides and unstable slopes. Such studies would lead to an improved understanding of slope deformation mechanisms with benefits for future slope hazard and risk assessment.

Acknowledgments

We gratefully acknowledge BC Hydro for providing access to the database and logistic support during the field work. Thanks to Dr. Jim Hazzard (Itasca) for the online support with some advanced features for numerical modelling in 3DEC. Two anonymous reviewers provided feedback and comments that improved the quality of the paper.

References

Adhikary, D.P., Dyskin, A.V., Jewell, R.J., Stewart, D.P., 1997. A study of the mechanism of flexural toppling failure of rock slopes. *Rock Mech. Rock Eng.* 30(2), 75-93. https://doi.org/10.1007/BF01020126

Agliardi, F., Crosta, G.B., Frattini, P., Malusà, M.G., 2013a. Giant non-catastrophic landslides and the long-term exhumation of the European Alps. *Earth Planet. Sci. Lett.* 365, 263–274. https://doi.org/10.1016/j.epsl.2013.01.030

Agliardi, F., Crosta, G.B., Meloni, F., Valle, C., Rivolta, C., 2013b. Structurally-controlled instability, damage and slope failure in a porphyry rock mass. *Tectonophysics* 605, 34-47. https://doi.org/10.1016/j.tecto.2013.05.033

Agliardi, F., Crosta, G.B., Zanchi, A., Ravazzi, C., 2009. Onset and timing of deep-seated gravitational slope deformations in the eastern Alps, Italy. *Geomorphology* 103, 113–129. https://doi.org/10.1016/j.geomorph.2007.09.015

Alejano, L.R., Alonso, E., 2005. Considerations of the dilatancy angle in rocks and rock masses. *Int. J. Rock Mech. Min. Sci.* 42, 481–507. https://doi.org/10.1016/j.ijrmms.2005.01.003

Ambrosi, C., Crosta, G.B., 2006. Large sackung along major tectonic features in the Central Italian Alps. *Eng. Geol.* 83(1-3), 183-200. https://doi.org/10.1016/j.enggeo.2005.06.031

Andrieux, P., Zhu, H., Labrie, D., Doucet, C., Lampron, S. and Fleury, D. (2004). Determination and validation of the rock mass post-peak mechanical properties for a 3DEC strain-softening model of the 680 Sill Pillar at Louvicourt Mine, in: Heinz, K. (ed.) *Numerical Modeling of Discrete Materials in Geotechnical Engineering, Civil Engineering, and Earth Sciences*. Taylor & Francis Routledge.

Badger, T.C., 2002. Fracturing within anticlines and its kinematic control on slope stability. *Environ. Eng. Geosci.* 8, 19–33. https://doi.org/10.2113/gseegeosci.8.1.19

Badr, S., Ozbay, U., Kieffer, S. and Salamon, M.D.G., 2003. Three-dimensional strain softening modeling of deep longwall coal mine layouts, in: R. Brummer, Andirieux, P., Detournay, C. and Hart, R. (eds.), *Third International Symposium on FLAC and FLAC3D Numerical Modelling in Geomechanics*, 21-24 October, Sudbury, Ontario, Canada, pp. 233–239.

BC Hydro, 1974. Revelstoke project, Downie Slide investigation, summary of the 1973 exploration program. Report 725. (Unpublished)

BC Hydro, 2010. Downie Slide drainage improvement project. Stability reassessment. Report E798. (Unpublished)

Bonzanigo, L., Eberhardt, E., Loew, S., 2007. Long-term investigation of a deep-seated creeping landslide in crystalline rock. Part I. Geological and hydromechanical factors controlling the Campo Vallemaggia landslide. *Can. Geotech. J.* 44, 1157-1180. https://doi.org/10.1139/T07-043

Brideau, M.-A., Stead, D., Kinakin, D., Fecova, K., 2005. Influence of tectonic structures on the Hope Slide, British Columbia, Canada. *Eng. Geol.* 80, 242–259. https://doi.org/10.1016/j.enggeo.2005.05.004

Brown, R.L., Psutka, J.F., 1980. Structural and stratigraphic setting of the Downie slide, Columbia River valley, British Columbia. *Can. J. Earth Sci.* 17, 698–709. https://doi.org/10.1139/e80-067

Brown, R.L., Read, P.B., 1983. Shuswap terrane of British Columbia: A Mesozoic "core complex." *Geology* 11 (3), pp. 164-168. https://doi.org/10.1130/0091-7613(1983)11<164:STOBCA>2.0.CO;2

Carbonel, D., Gutiérrez, F., Linares, R., Roqué, C., Zarroca, M., McCalpin, J., Guerrero, J., Rodríguez, V., 2013. Differentiating between gravitational and tectonic faults by means of geomorphological mapping, trenching and geophysical surveys. The case of the Zenzano Fault (Iberian Chain, N Spain). *Geomorphology* 189, 93–108. https://doi.org/10.1016/j.geomorph.2013.01.020

Chigira, M., 1992. Long-term gravitational deformation of rocks by mass rock creep. *Eng. Geol.* 32, 157–184. https://doi.org/10.1016/0013-7952(92)90043-X

Clayton, A., Stead, D., Kinakin, D., Wolter, A., 2017. Engineering geomorphological interpretation of the Mitchell Creek Landslide, British Columbia, Canada. *Landslides* 14, 1655–1675. https://doi.org/10.1007/s10346-017-0811-1

Donati, D., 2019. The characterization of slope damage using an integrated remote sensing-numerical modelling approach. Ph.D. Thesis. Simon Fraser University.

Donati, D., Stead, D., Lato, M., Gaib, S., 2020. Spatio-temporal characterization of slope damage: insights from the Ten Mile Slide, British Columbia, Canada. *Landslides*. https://doi.org/10.1007/s10346-020-01352-3

Eberhardt, E., Bonzanigo, L., Low, S., 2007. Long-term investigation of a deep-seated creeping landslide in crystalline rock. Part II. Mitigation measures and numerical modelling of deep drainage at Campo Vallemaggia. *Can. Geotech. J.* 44, 1181-1199. https://doi.org/10.1139/T07-044

ESRI, 2017. ArcGIS 10.6.

Golden Software, 2016. Surfer 14.

Ganerød, G.V., Grøneng, G., Rønning, J.S., Dalsegg, E., Elvebakk, H., Tønnesen, JF., Kveldsvik, V., Eiken, T., Blikra, L.H., Braathen, A., 2008. Geological model of the Åknes rockslide, western Norway, *Eng. Geol.* 102(1–2), 1-18. https://doi.org/10.1016/j.enggeo.2008.01.018

Glastonbury, J., Fell, R., 2008. Geotechnical characteristics of large slow, very slow, and extremely slow landslides. *Can. Geotech. J.* 45, 984-1005. https://doi.org/10.1139/T08-021

Hajiabdolmajid, V., Kaiser, P.K., 2002. Slope stability assessment in strain-sensitive rocks, in: ISRM (ed.) *Proceedings of the ISRM International Symposium. EUROCK 2002*, 25-27 November, Madeira, Portugal, pp. 237–244.

Hermanns, R.L., Fauqué, L., Wilson, C.G.J., 2015. 36^{Cl} terrestrial cosmogenic nuclide dating suggests Late Pleistocene to Early Holocene mass movements on the south face of Aconcagua Mountain and in the Las Cuevas–Horcones valleys, Central Andes, Argentina. *Geol. Soc. London, Spec. Publ*. 399, 345–368. https://doi.org/10.1144/SP399.19

Hoek, E., Brown, E.T., 1997. Practical estimates of rock mass strength. *Int. J. Rock Mech. Min. Sci.* 34, 1165–1186. https://doi.org/10.1016/S1365-1609(97)80069-X

Humair, F., Pedrazzini, A., Epard, J.L., Froese, C.R., Jaboyedoff, M., 2013. Structural characterization of Turtle Mountain anticline (Alberta, Canada) and impact on rock slope failure. *Tectonophysics* 605, 133–148. https://doi.org/10.1016/j.tecto.2013.04.029

739 Imrie, A.S., Moore, D.P., 1993. The Use of Rock Engineering to Overcome Adverse Geology at Revelstoke Dam, in:
740 Hoek, E. (ed.), *Surface and Underground Project Case Histories*. Elsevier. pp. 701–725.
741 https://doi.org/10.1016/B978-0-08-042068-4.50037-5

742 Imrie, A.S., Moore, D.P., Enegren, E.G., 1992. Performance and maintenance of the drainage system at Downie
743 Slide, in: Bell (Ed.), *Landslides: Proceedings of the Sixth International Symposium*, 10-14 February,
744 Christchurch, New Zealand, pp. 751–757.

745 Itasca Consulting Group, 2000. FLAC 4.

746 Itasca Consulting Group, 2016a. 3DEC 5.2.

747 Itasca Consulting Group, 2016b. Griddle 1.0.

748 Jaboyedoff, M., Penna, I., Pedrazzini, A., Baroň, I., Crosta, G.B., 2013. An introductory review on gravitational-
749 deformation induced structures, fabrics and modeling. *Tectonophysics* 605, 1–12.
750 https://doi.org/10.1016/j.tecto.2013.06.027

751 Kalenchuk, K.S., Diederichs, M.S., Hutchinson, D.J., 2012. Three-dimensional numerical simulations of the Downie
752 Slide to test the influence of shear surface geometry and heterogeneous shear zone stiffness. *Comput. Geosci.*
753 16, 21–38. https://doi.org/10.1007/s10596-011-9245-3

754 Kalenchuk, K.S., Hutchinson, D.J., Diederichs, M.S., 2009. Downie Slide - Interpretations of complex slope
755 mechanics in a massive, slow moving, translational landslide, in: Canadian Geotechnical Society (ed),
756 *Proceedings of the 62nd Canadian Geotechnical Conference GeoHalifax 2009*, 20-24 September, Halifax,
757 Canada, pp. 367–374.

758 Kalenchuk, K.S., Hutchinson, D.J., Diederichs, M.S., 2013a. Geomechanical interpretation of the Downie Slide
759 considering field data and three-dimensional numerical modelling. *Landslides* 10, 737–756.
760 https://doi.org/10.1007/s10346-012-0363-3

761 Kalenchuk, K.S., Hutchinson, D.J., Diederichs, M.S., 2013b. Downie Slide: Numerical simulation of groundwater
762 fluctuations influencing the behaviour of a massive landslide. *Bull. Eng. Geol. Environ.* 72, 397–412.
763 https://doi.org/10.1007/s10064-013-0484-5

764 Kjelland, N.H., 2004. Slope stability analysis of Downie Slide: numerical modelling and GIS data analysis for
765 geotechnical decision support. M.Sc. Thesis. Queen's University.

766 Leith, K.J., 2012. Stress development and geomechanical controls on the geomorphic evolution of alpine valleys.
767 Ph.D. Thesis. ETH Zurich.

768 Macfarlane, D.F., 2009. Observations and predictions of the behaviour of large, slow-moving landslides in schist,
769 Clyde Dam reservoir, New Zealand. *Eng. Geol.* 109, 5-15. https://doi.org/10.1016/j.enggeo.2009.02.005

770 Moore, D.P., 1993. Rock slopes and reservoirs – lesson learned, in: Vancouver Geotechnical Society (ed), *13°*
771 *Annual Vancouver Geotechnical Society Symposium*, May 28, Vancouver, Canada. 18 p.

772 Moore, J.R., Gischig, V., Burjanek, J., Loew, S., Fäh, D., 2011. Site effects in unstable rock slopes: Dynamic
773 behavior of the Randa instability (Switzerland). *Bull. Seismol. Soc. Am.* 101, 3110–3116.
774 https://doi.org/10.1785/0120110127

NASA-NGA, 2014. SRTM 1 Arc-Second Global, Version 3. NASA EOSDIS Land Processes DAAC, USGS Earth Resources Observation and Science (EROS) Center, Sioux Falls, South Dakota (https://lpdaac.usgs.gov), accessed October 2019, at https://earthexplorer.usgs.gov/.

O'Brein, G.A., Cox, S.C., Townend, J., 2016. Spatially and temporally systematic hydrologic changes within large geoengineered landslides, Cromwell Gorge, New Zealand, induced by multiple regional earthquakes. *J. Geophys. Res. B: Solid Earth* 121, 8750-8773. https://doi.org/10.1002/2016JB013418

Oppikofer, T., Saintot, A., Hermanns, R.L., Böhme, M., Scheiber, T., Gosse, J., Dreiås, G.M., 2017. From incipient slope instability through slope deformation to catastrophic failure — Different stages of failure development on the Ivasnasen and Vollan rock slopes (western Norway). *Geomorphology* 289, 96–116. https://doi.org/10.1016/j.geomorph.2017.03.015

Paronuzzi, P., Bolla, A., 2015. Gravity-induced rock mass damage related to large en masse rockslides: Evidence from Vajont. *Geomorphology* 234, 28–53. https://doi.org/10.1016/j.geomorph.2015.01.008

Piteau, D.R., Ylrea, F.H., Blown, I.G., 1978. Downie Slide, Columbia River, British Columbia, Canada, in: Voight, B. (ed.), *Rockslides and Avalanches, Volume 1*. pp. 365–392.

Preisig, G., Eberhardt, E., Smithyman, M., Preh, A., Bonzanigo, L., 2016. Hydromechanical rock mass fatigue in deep-seated landslides accompanying seasonal variations in pore pressures. *Rock Mech. Rock Eng.* 49, 2333–2351. https://doi.org/10.1007/s00603-016-0912-5

Riva, F., Agliardi, F., Amitrano, D., Crosta, G.B., 2018. Damage-based time-dependent modeling of paraglacial to postglacial progressive failure of large rock slopes. *J. Geophys. Res. Earth Surf.* 123, 124–141. https://doi.org/10.1002/2017JF004423

Robert McNeel & Associates, 2015. Rhinoceros 5.

Rocscience, 2019. DIPS version 7.

Saintot, A., Henderson, I.H.C., Derron, M.-H., 2011. Inheritance of ductile and brittle structures in the development of large rock slope instabilities: examples from western Norway. *Geol. Soc. London, Spec. Publ.* 351, 27–78. https://doi.org/10.1144/SP351.3

Semenza, E., Ghirotti, M., 2000. History of the 1963 Vaiont slide: the importance of geological factors. *Bull. Eng. Geol. Environ.* 59, 87–97. https://doi.org/10.1007/s100640000067

Stantec Inc., 2009. Bedrock and surficial geology of Downie Slide, final report. (Unpublished)

Stead, D., Eberhardt, E., 2013. Understanding the mechanics of large landslides. *Italian Journal of Engineering Geology and Environment - Book Series* (6), 85–112. https://doi.org/10.4408/IJEGE.2013-06.B-07

Stead, D., Eberhardt, E., 1997. Developments in the analysis of footwall slopes in surface coal mining. *Eng. Geol.* 46, 41–61. https://doi.org/10.1016/S0013-7952(96)00084-1

Stead, D., Wolter, A., 2015. A critical review of rock slope failure mechanisms: the importance of structural geology. *J. Struct. Geol.* 74, 1–23. https://doi.org/10.1016/j.jsg.2015.02.002

Westin, A.M., 2017. Downie Slide: an integrated remote sensing approach to characterization of a very slow moving landslide. M.Sc. Thesis. Simon Fraser University.

Whalley, W.B., 1974. The mechanics of high-magnitude low-frequency rock failure. *Read. Geogr. Pap.* 27.

Wolter, A., Stead, D., Clague, J.J., 2014. A morphologic characterisation of the 1963 Vajont Slide, Italy, using long-range terrestrial photogrammetry. *Geomorphology* 206, 147–164. https://doi.org/10.1016/j.geomorph.2013.10.006

Zangerl, C., Eberhardt, E., Perzlmaier, S., 2010. Kinematic behaviour and velocity characteristics of a complex deep-seated crystalline rockslide system in relation to its interaction with a dam reservoir. *Eng. Geol.* 112(1-4), 53-67. https://doi.org/10.1016/j.enggeo.2010.01.001

Zipf, K., 2007. Numerical modeling procedures for practical coal mine design, in: Mark, C., Pakalnis, R., and Tuchman, R. J. (eds.). *Proceedings of the International Workshop on Rock Mass Classification in Underground Mining*, 1. pp. 153–160.